Fan et al. *Microsystems & Nanoengineering* (2024)10:154
https://doi.org/10.1038/s41378-024-00791-5

Microsystems & Nanoengineering
www.nature.com/micronano

REVIEW ARTICLE Open Access

Graphene MEMS and NEMS

Xuge Fan[1,2,3]✉, Chang He[1], Jie Ding[3]✉, Qiang Gao[1], Hongliang Ma[1,3], Max C. Lemme[4,5] and Wendong Zhang[6,7]✉

Abstract

Graphene is being increasingly used as an interesting transducer membrane in micro- and nanoelectromechanical systems (MEMS and NEMS, respectively) due to its atomical thickness, extremely high carrier mobility, high mechanical strength, and piezoresistive electromechanical transductions. NEMS devices based on graphene feature increased sensitivity, reduced size, and new functionalities. In this review, we discuss the merits of graphene as a functional material for MEMS and NEMS, the related properties of graphene, the transduction mechanisms of graphene MEMS and NEMS, typical transfer methods for integrating graphene with MEMS substrates, methods for fabricating suspended graphene, and graphene patterning and electrical contact. Consequently, we provide an overview of devices based on suspended and nonsuspended graphene structures. Finally, we discuss the potential and challenges of applications of graphene in MEMS and NEMS. Owing to its unique features, graphene is a promising material for emerging MEMS, NEMS, and sensor applications.

Introduction

Graphene was experimentally discovered in 2004[1,2] and has since attracted substantial attention in fundamental and applied research by the physics, chemistry, and materials science communities. Monolayer graphene consists of a one-atom-thick sheet of tightly packed carbon atoms that are bonded together in a hexagonal honeycomb lattice. Monolayer graphene is the thinnest known material (~0.335 nm thick) and is extremely strong, chemically stable, and exceptionally conductive[3]. Owing to its high thickness and unique mechanical and electrical properties[4–6], graphene is an extremely promising material for use as an electromechanical transducer in nanoelectromechanical systems (NEMS); as an electromechanical transducer, graphene could substantially reduce the device footprint while providing improved device performance. Furthermore, in monolayer graphene, all the atoms are directly exposed to the environment, thereby impacting the electrical properties of all the atoms of the monolayer graphene; thus, graphene is especially interesting for sensing applications. In addition, because of its planar geometry, graphene is easily compatible with standard lithographic processing. An obvious advantage is that although graphene is intrinsically nanoscale, it can be patterned via standard lithographic processes at the wafer scale.

Graphene is available in the form of large sheets and can be placed on top of various surfaces. Furthermore, graphene can be self-suspended in atomically thick membranes or beams. In addition, graphene can be suspended together with polymers or other membranes. Compared with other carbon-based nanomaterials, such as carbon nanotubes, a prominent advantage of using graphene for practical device applications is that the widely available planar semiconductor processing infrastructure can be used for manufacturing graphene devices. Many practical applications of graphene in areas such as electronics (e.g., transistors, ultrathin and optically transparent electrodes, supercapacitors, and spintronics)[7–9], photonics (e.g., photodetectors and optical modulators)[7,10], and composite materials (e.g., polymer reinforcements, lubricants, and coolants)[7,11–13] have been explored in terms of the unique electrical, optical, and mechanical properties of graphene.

Because of its unique properties, graphene is also an extremely attractive material for micro- and nanoelectromechanical systems (MEMS and NEMS, which, in this review, are collectively referred to as "NEMS"). Initially,

Correspondence: Xuge Fan (xgfan@bit.edu.cn) or Jie Ding (jie.ding@bit.edu.cn) or Wendong Zhang (wdzhang@nuc.edu.cn)
[1]Advanced Research Institute of Multidisciplinary Sciences, Beijing Institute of Technology, 100081 Beijing, China
[2]Center for Interdisciplinary Science of Optical Quantum and NEMS Integration, School of Physics, Beijing Institute of Technology, 100081 Beijing, China
Full list of author information is available at the end of the article

graphene was used in NEMS for fundamental studies on resonant structures[14] and in gas sensors[15]. Graphene has only recently been widely studied in different NEMS and sensor applications[16,17]. We believe that there are many opportunities to exploit the unique properties of graphene in NEMS devices. Graphene-based NEMS resonators were provided in review papers[18–20], and brief summaries of graphene in MEMS and NEMS were given in the literature[21,22]. In addition, NEMS sensors based on suspended 2D materials were comprehensively reviewed in 2020[23]. Graphene-based photonic detectors have been comprehensively reviewed recently[24,25] and are not included here.

Compared with previous work, this review paper provides a broad overview of various graphene-based NEMS and devices that have been reported in the literature. We discuss the relevant properties of graphene and present key manufacturing technologies for enabling graphene-based NEMS structures. First, we show different graphene materials, their properties, and different transduction mechanisms for NEMS devices. Consequently, we discuss various graphene manufacturing and integration techniques for NEMS applications, including methods for transferring and patterning graphene, electrical contacting, and realizing suspended graphene. Finally, we summarize different MEMS and NEMS devices based on suspended and nonsuspended graphene structures, such as various types of pressure sensors; resonators; switches; mass sensors; accelerometers; microphones and loudspeakers; gas sensors; hall sensors; and flexible devices, including transparent electrodes, strain sensors, pressure sensors, and audio-emitting and receiving devices.

Graphene properties

Graphene is a two-dimensional material consisting exclusively of carbon atoms that are densely packed in a regular atomic-scale hexagonal pattern. Each atom in a graphene sheet has four bonds: one σ bond with each of its three neighbors and one π-bond that is oriented out of plane. The atoms in graphene are spaced ~0.142 nm from each other (i.e., the length of the molecular bonds between the carbon atoms), and the thickness of a layer of graphene is ~0.34 nm (i.e., the spacing between two graphene sheets when stacked on top of each other). In general, graphene is a monolayer, bilayer, or multiple layers ($n < 10$) of carbon atoms bonded by strong covalent bonds within a layer (sp^2 hybridization in a hexagonal lattice and partial filling of π-orbitals above and below the plane of the sheet) with weak van der Waals bonds between neighboring layers. Many reported properties of graphene are exceptional[26], including an intrinsic Young's modulus of 1 TPa[5], an intrinsic strength of 130 GPa[5], room-temperature electron mobility of up to $2.5 \times 10^5\ cm^2\ V^{-1}s^{-1}$ [27], a high thermal conductivity of above $3000\ W\ mK^{-1}$ [28], an excellent transparency and uniform optical absorption of ≈2.3% in a wide wavelength range[29], an impermeability to gases[30], a stretchability of up to ~20%[31], and high compatibility with high densities of electric current[32]. Furthermore, graphene can strongly adhere to SiO_2 surfaces[33] and can stably exist in suspended membranes even with a thickness of one atom layer[34]. In addition, graphene can be readily chemically functionalized[35]. Therefore, graphene is a promising material for NEMS applications. Notably, some of these extreme properties can be measured only in high-quality graphene samples, such as mechanically exfoliated graphene without grain boundaries[1] or graphene on hexagonal boron nitride[27,36].

Different methods are used to produce graphene; they include mechanical exfoliation[1,2,14], liquid-phase exfoliation[37–40], chemical vapor deposition (CVD)[41–43], and epitaxial methods[44,45]. The mechanical exfoliation of very high-quality graphene flakes is not easily scalable, and the placement of the resulting μm-scale flakes cannot be adequately controlled for large-scale device applications. For many practical MEMS and sensor applications, CVD graphene is one of the most attractive options. CVD graphene is typically deposited on a support substrate, such as a Cu or Ni foil, from which CVD graphene can be transferred to a variety of other substrate surfaces. CVD graphene on Cu or Ni foils is relatively inexpensive and widely available from commercial suppliers, such as the Beijing Graphene Institute (China), Graphenea Nanomaterials (Spain), Graphene-Supermarket (USA), 6Carbon Technology (Shenzhen) (China), and many others (2D Layer (USA), 2D Semiconductors (USA), etc.). A variety of substrate sizes are available (e.g., $10 \times 10\ mm^2$ or 100 mm diameter wafer foils), with relatively uniform and high-quality monolayer graphene. CVDs are typically polycrystalline; i.e., they are composed of monocrystalline grains of varying orientations joined by grain boundaries[46–48]. The properties of CVD graphene strongly depend on the material quality; the substrate material on which the graphene sheet is placed; and the graphene grain size, which is typically approximately a few μm to tens of μms[47]. Compared with that of monocrystalline graphene, the electrical properties of polycrystalline graphene may be strongly impacted by the grain boundaries. And electrical and mechanical properties depending on the lattice may not be present in CVD graphene samples that consist of grains and grain boundaries. Typical technologically relevant material properties of polycrystalline CVD graphene are listed in Table 1 [46], along with the best reported material properties of high-quality graphene[26]. Other available forms of graphene include (1) graphene sheets, which are grown on SiC substrates (i.e., grown via epitaxy); (2) graphene flakes in liquid solution ranging from nm to μm, which are produced through

Table 1 Relevant properties of graphene for MEMS and NEMS applications

Graphene Typical Properties	Polycrystalline CVD graphene	Exfoliated graphene
Young's modulus	1.02 TPa [259]	1.02 TPa [5]
Fracture strain	Up to 20% [31]	Up to 30% [5,319,320]
Electrical conductivity	On SiO_2: 4050 cm^2/Vs [42] On h-BN: 350,000 cm^2/Vs[321] Suspended: 15,000 cm^2/Vs[322]	On SiO_2: 15,000 cm^2/Vs[2] On h-BN: 275,000 cm^2/Vs; (T = RT): 120,000 cm^2/Vs[323] Suspended: 185,000 cm^2/Vs[324]
Sheet resistance	72 Ω/sq[325] Few hundred Ω/sq to > 10^4 Ω/sq[326]	Few hundred Ω/sq to >10^4 Ω/sq[326]
Thermal conductivity	Suspended: ~1500–5000 W/mK[327]	Suspended: ~4840–5300 W/mK[328,329]
Temperature coefficient of expansion	7×10^{-6} K^{-1} [330]	7×10^{-6} K^{-1} [331]
Permeability	Gases or ions might permeate grain boundaries or defects; therefore, multilayer CVD graphene is better[332]	Impermeable, even against helium[30]
Gauge factor	3 (suspended drum)[34] >300 (nanographene films)[58]	1.9 (suspended beam)[60] 150 (on SiO_2)[67]

liquid-phase exfoliation and can be coated on the surface, resulting in the coating with dispersed, randomly overlapping graphene flakes; and (3) reduced-graphene oxide (GO), which is produced via laser scribing (this process results in loosely stacked graphene layers, graphene aerogels, and graphene foams[26,49]).

Transduction mechanisms of graphene for NEMS

Many transduction mechanisms in graphene can be used in NEMS and sensor devices; these mechanisms include the piezoresistive effect in graphene, electrostatic sensing (including capacitive and transconductance change by a gate electrode), electrostatic actuation with graphene electrodes, resonant and optical transduction, Hall effects, and resistance changes in graphene due to surface interactions. Notably, electrical signals from graphene is extremely sensitive to various environmental parameters. Hence, parameters such as small changes in the humidity of the surrounding air in contact with the graphene[50–53], gases[51,52,54], temperature[55], or electromagnetic fields from nearby circuits impact the electronic signals of graphene devices. Therefore, to ensure the reliability of electrical signals from practical graphene-based device applications, all critical environmental parameters must be controlled, and the graphene must be carefully shielded from environmental influences, such as electromagnetic fields and changes in environmental gas composition. For example, graphene can be encapsulated by h-BN, Si_3N_4, Al_2O_3, or poly(methyl methacrylate) (PMMA)-based polymers. Each of the transduction mechanisms is discussed in the following subsections.

Piezoresistive transduction

Graphene has been demonstrated to have a piezoresistive effect; i.e., the mechanical strain induced in graphene results in a change in the graphene resistance[56,57]. Two types of basic functional structures based on the piezoresistive effect of graphene are shown in Fig. 1a, b [34,58]. The first type is a suspended graphene membrane that can act at the same time as the membrane and strain gauge (Fig. 1a)[34]. The second type is a graphene strain gauge that can be placed on a substrate or a membrane (Fig. 1b)[58,59]. For exfoliated and CVD graphene with typical grain sizes of a few μm, piezoresistive gauge factors, which are the ratios of the relative resistance change to the mechanical strain, have commonly been reported to be ~1.9 to 8.8 (Fig. 1c–f)[59–64]. In such graphene sheets, the resistance change of graphene is caused by external strain-induced changes in the electronic band structure in graphene. Theoretical analysis and reported measurements suggest that the direction of the strain in relation to the graphene crystal lattice orientation has no significant influence on the gauge factor, and uniaxial and biaxial strain in graphene result in similar gauge factors (Fig. 1g)[65]. Furthermore, the reported piezoresistive gauge factors of bilayer graphene structures are similar to those of monolayer graphene (Fig. 1h)[66]. However, the piezoresistive properties of graphene are associated with the graphene type, the graphene quality (e.g., gain size and density), the structure (e.g., suspended graphene membrane and graphene placed on a substrate), and the materials that are in contact with the graphene (e.g., substrate and passivation layers).

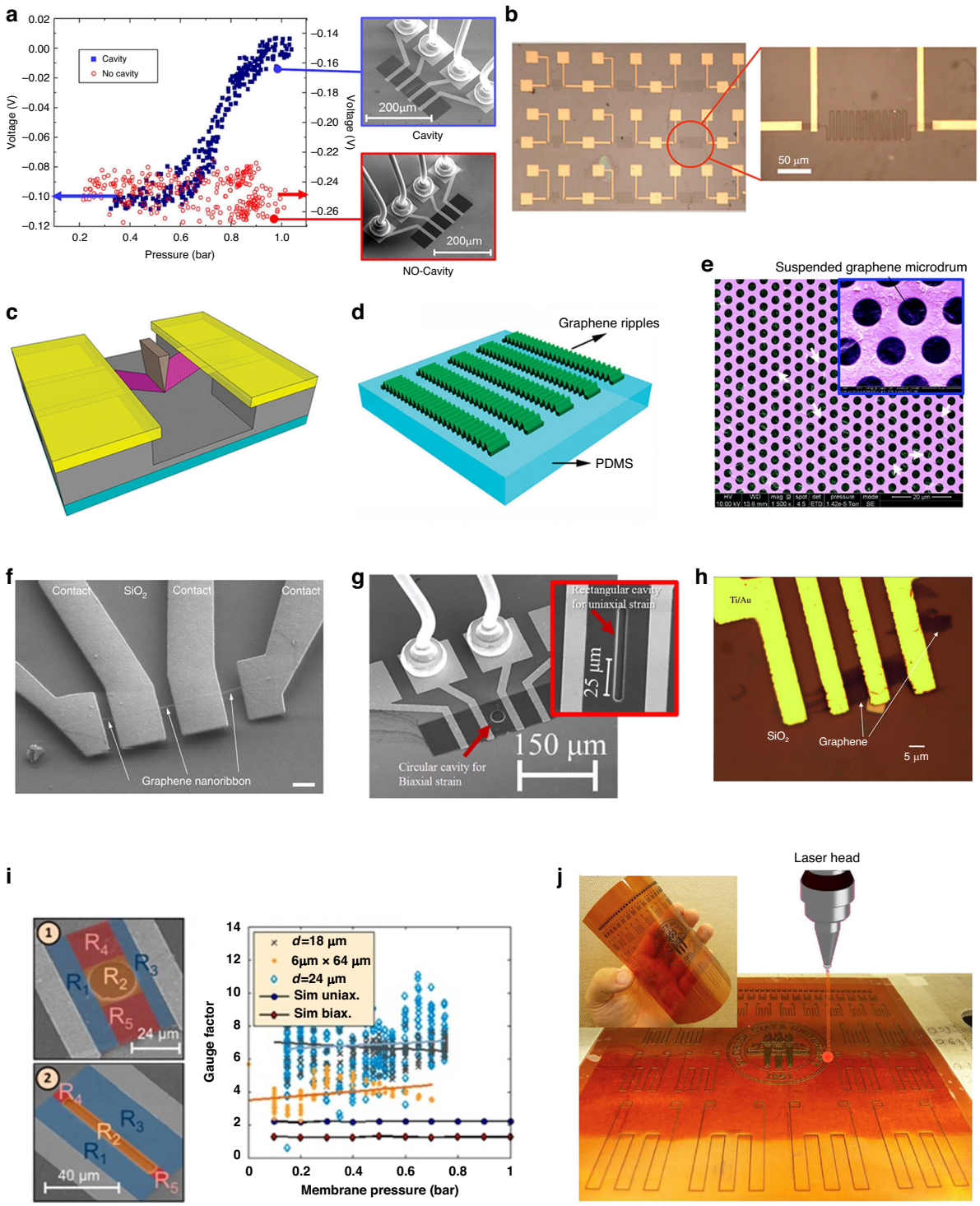

Fig. 1 Piezoresistive transduction of graphene. a A piezoresistive NEMS pressure sensor based on a suspended monolayer graphene membrane[34]. **b** Nanographene-based strain sensor devices[58]. **c** Nanoindentation experiments performed on suspended graphene devices for measuring strain and gauge factors[60]. **d** Buckled graphene ribbons on a Polydimethylsiloxane (PDMS) substrate[63]. **e** Arrays of suspended graphene microdrums[59]. **f** A graphene nanoribbon device[64]. **g** Biaxial strain in suspended graphene membranes[65]. **h** An optical microscope image of a monolayer graphene sheet on a SiO_2 surface for measuring gauge factors[66]. **i** Extracted gauge factors of both uniaxially and biaxially strained graphene membranes[70]. **j** Direct laser writing–fabricated graphitic sensor patterns on a polyimide film[73]. Figures reproduced with permission from refs. [34,58–60,63–66,70,73]

There have been isolated reports of very high gauge factors in graphene; these factors range from 150[67] to 17980[68]. However, the exact graphene materials used were not specified in the original or follow-up studies, which yielded comparable results. Here, the piezoresistive effect of graphene is caused by mechanical strain in the graphene, which changes the electronic band structure. The piezoresistive behavior of graphene is a superposition of carrier density and carrier mobility modification, where the latter dominates. The piezoresistive behavior is independent of the crystallographic orientation, and the gauge factor is independent of the doping concentration. For small strains, the intrinsic piezoresistive gauge factor of graphene is largely invariant in strain magnitude (Fig. 1i)[34,61,69,70].

Large gauge factors have also been reported for coatings with randomly overlapping graphene flakes, for loosely stacked graphene layers prepared by reducing GO via laser scribing, and for graphene-based composites and graphene films on soft substrates. For example, gauge factors of over 300 can be obtained from synthesized nanographene films (which comprise densely packed nanographene islands) by controlling the piezoresistive response of these films by changing their growth parameters[58]. Additionally, gauge factors of more than 600 can be achieved from nanographene films[71]. Graphene-based thin-film strain gauges that produce solution-processed overlapping graphene flakes via spray deposition have high and tunable gauge factors with maximum values greater than 150[72]. A high gauge factor of ~112 for porous graphitic structures can be achieved by direct laser writing from polyimide (Fig. 1j)[73]. A gauge factor of ~11.4 for a graphene/epoxy composite within the range of 1000 microstrains has been reported[74]. More interestingly, depending on the strain level, high gauge factors ranging from 10^3 to 10^6 for graphene woven fabrics, including woven graphene microribbons, have been reported because of their woven mesh configuration, high-density crack formation, and propagation mechanical deformation[75]. A strain sensor made of a vinyl-ester polymer composite filled with multilayer graphene nanoplatelets has a gauge factor of ~45[76], whereas percolative film devices based on *N*-methyl-2-pyrrolidone (NMP)/graphene flakes on flexible plastic substrates have gauge factors ranging from 10 to 100 [72].

Electrostatic transduction

Electrostatic sensing commonly includes both capacitance changes between moving and fixed plates as their distance and position are changed or media are replaced and transconductance changes by a gate electrode. A high capacitance sensitivity of the graphene membrane for pressure sensing was achieved[77]; this sensitivity is 770% greater than that of frequently used silicon-based membranes. Graphene field-effect transistors are typical devices based on transconductance changes caused by gate electrodes. Graphene, with its novel and electron–hole symmetric band structure and high carrier mobilities and thermal velocities, has gained much attention for overcoming the limitations of Moore's law and 'beyond CMOS' devices. Although pristine monolayer graphene is a gapless semiconductor and current control by gate electrodes is challenging, off-state leakage currents are high, and the current does not readily saturate with the drain voltage. Several reviews on graphene-based field-effect transistors have been published in recent years[78–81].

One of the most popular actuation mechanisms used in MEMS/NEMS is electrostatic actuation, which is realized by the electrostatic force (attraction) between moving and fixed plates by applying a voltage between them. For example, flexible strain sensors made of graphene flakes with electrostatic actuation have a mechanical resonance frequency of ~136 MHz under ambient conditions[82]. One typical application of MEMS/NEMS electrostatic actuators is nanoelectromechanical switches, which use electrostatic forces to mechanically deflect the active element into physical contact with an electrode. Graphene has a high Young's modulus, high atomic thickness, and high electron mobility, thus making graphene a promising candidate material for NEMS switches. As shown in Fig. 2a, the graphene NEMS switch resulted in minimal electrical leakage, a sharp switching response, a low actuation voltage, and a high on/off ratio[83–87]. Typically, the heavily doped silicon substrate is used as the actuation electrode, thus causing the graphene NEMS switch to suffer from a relatively large pull-in voltage (>10 V) mainly because of the thick, inevitable dielectric gap[88]. To reduce the pull-in voltage, a local actuation gate electrode is normally needed. Both the structures of the graphene cantilever and doubly clamped graphene can be used for graphene MEMS/NEMS switches (Fig. 2b–d)[89–93].

Resonant transduction

The low areal mass density and high tension of graphene membranes enable graphene-based resonant structures to achieve very high resonance frequencies. Since loudspeakers and microphones can provide only a flat-band response below the lowest resonance mode, graphene speakers[94], and microphones[95] could benefit the transduction of ultrasound. The thermal-mechanical pressure noise p_{noise} in a microphone is given by $p_{noise} = \sqrt{\frac{4 k_B T \sqrt{km}}{A^2 Q}}$, where k denotes the spring constant, m denotes the mass, and A denotes the area of the membrane. This equation shows that the increase in noise due to a reduction in the area of the microphone

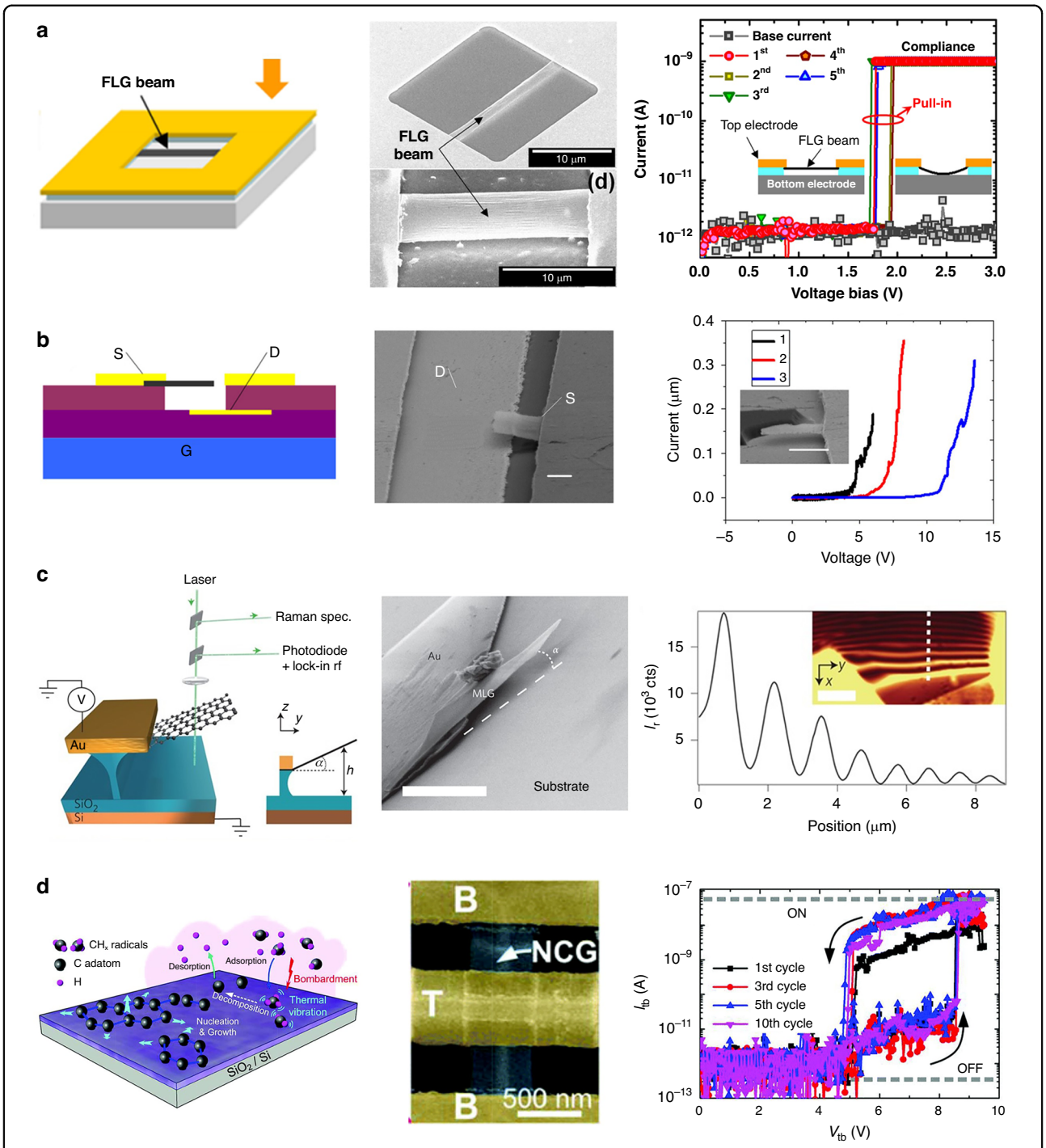

Fig. 2 Electrostatic transduction of graphene. a A suspended few-layer graphene beam electromechanical switch[84]. **b** An MLG cantilever overhanging silicon oxide[90]. **c** Nanoelectromechanical switches based on nanocrystalline graphene directly deposited on insulating substrates[93]. **d** A 3-terminal nanoswitch based on a graphene cantilever[89]. Figures reproduced with permission from refs. [84,89,90,93]

membrane can be compensated for by the reduced mass and spring constant of the graphene membranes.

A method for resonant pressure sensing is based on suspended graphene membranes, which do not require a hermetically sealed cavity; instead, pressure is measured by high-frequency compression of the gas in a "squeeze film" between the graphene membrane and the substrate[96]. Because of the high compression frequency, the gas has no time to escape, even in a nonhermetic cavity with a venting channel[96]. As a result, the trapped gas acts as a

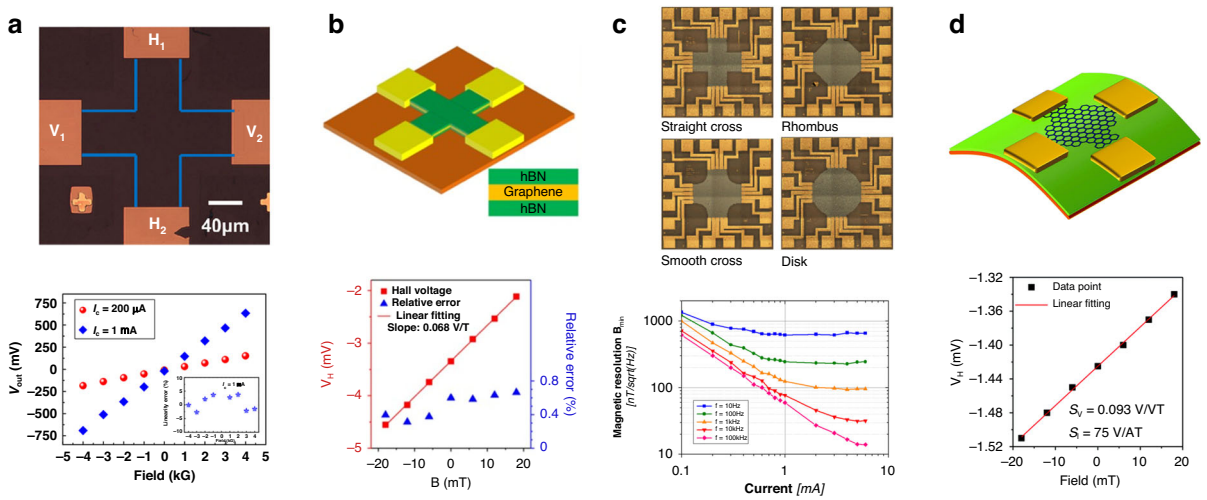

Fig. 3 Transduction based on the Hall effect. a A graphene Hall effect sensor[106]. **b** A graphene Hall effect sensor encapsulated by h-BN[107]. **c** Quasifree-standing hydrogen-intercalated monolayer graphene Hall effect sensors with different shapes and room-temperature magnetic resolutions[109]. **d** A flexible Hall sensor based on graphene[110]. Figures reproduced with permission from refs. [106,107,109,110]

pressure-dependent spring that increases the resonant frequency of the graphene membrane.

Optical transduction of graphene NEMS resonators has been used[97–100]. Typically, an intensity-modulated laser is used to periodically heat the suspended graphene via optical absorption, which photothermally drives the motion of the suspended graphene via periodic contraction/expansion. Another laser is used for detection because of the interference caused by the multireflection of light within the graphene resonators[18,19]. Specifically, a laser reflects from the suspended graphene and simultaneously reflects off the substrate after it passes through the suspended graphene. As the suspended graphene vibrates, the space between the suspended graphene and the substrate changes correspondingly, thereby ultimately changing the interferometry condition of the graphene resonators. The displacement and related parameters of the graphene resonator can be obtained by measuring the intensity modulation of the reflected light. The light signal is then converted into an electrical signal by using a fast photodetector. This technique has minimal requirements for the device structure (e.g., not requiring electrodes) and material properties (e.g., no need to be conductive) and is suitable for quickly measuring NEMS resonators made from graphene and emerging 2D materials. Furthermore, this technique is very sensitive to the motion of graphene resonators and can measure the undriven thermomechanical resonance caused by the Brownian motion of the graphene device[14,19].

Transduction based on the Hall effect

The Hall effect refers to the generation of a voltage difference (Hall voltage) across an electrical conductor that is transverse to an electric current in the conductor and a magnetic field perpendicular to the current[101]. The Hall effect is a transducer mechanism whose output voltage varies in response to a magnetic field and can be used to measure the charge carrier density, charge carrier mobility, or magnetic field. The Hall element is a simple device structure that can be easily fabricated, and the performance of a Hall element depends mainly on the charge carrier mobility and density of the material[102]. Graphene, as an atomically thin 2D material, has very high charge carrier mobility and low charge carrier density at room temperature and is, therefore, a promising material for high-performance Hall sensors. As shown in Fig. 3, a typical cross-shaped graphene Hall element is a four-terminal device with two pairs of electrodes connected with four terminals of the graphene Hall cross, which are used for supplying current (current mode) or voltage (voltage mode) and measuring the Hall voltage[103]. A graphene Hall sensor can be used in either current mode or voltage mode. According to the Hall effect, when an external magnetic field B is applied perpendicular to the graphene surface, and a constant current (I) or a constant voltage (V) is supplied through the graphene channel, a Hall voltage (V_H) that is linearly related to the strength of the magnetic field is produced as follows[103–105]:

$$V_H = S_I \times I \times B \tag{1}$$

$$V_H = S_V \times V \times B \tag{2}$$

where S_I and S_V denote the current-related and voltage-related sensitivities, respectively, which are the key performance parameters of the graphene Hall elements. A simple derivation showing that the current- and voltage-related sensitivities of a graphene Hall element

correlate with carrier density or mobility can be expressed as[103–105]

$$S_I = \frac{1}{qn_s} \tag{3}$$

$$S_V = \frac{\mu W}{L} \tag{4}$$

where q denotes the elemental charge; W and L denote the width and length of the graphene channel, respectively; and n_s and μ denote the sheet carrier density and carrier mobility of the graphene channel, respectively. As Eqs. (3) and (4) show, the sensitivity of the graphene Hall element can be improved by decreasing the charge carrier density, increasing the charge carrier mobility, and optimizing the dimensions of the graphene active region. By changing the carrier density in the current mode, we can easily adjust the sensitivity of the graphene Hall sensors by using a gate voltage and by modifying the surface or substrate[104]. Graphene Hall elements generally feature high sensitivity (Fig. 3a, b)[103,106,107]. The combination of high sensitivity and low noise of graphene devices results in the higher resolution of the magnetic field (Fig. 3c)[108,109]. In addition to silicon-based substrates, graphene Hall elements can also be fabricated on flexible substrates (Fig. 3d)[110].

Other transduction mechanisms

Although unstrained pristine graphene does not exhibit piezoelectric properties, recent reports suggest that graphene exhibits piezoelectric behavior in certain configurations, such as applying strain or engineering graphene; this behavior can be caused by the charge transfer along a work function gradient introduced by the biaxial strain-engineered band structure of the suspended graphene membranes over the cavity[111] or associated with the chemical interaction of graphene's carbon atoms with the oxygen from the underlying SiO_2 grating substrates[112]. The piezoelectric transduction of strained or engineered graphene has potential applications in nanogenerators or actuators; however, the extent to which these properties can be used in practical device applications remains to be determined. In addition, suspended graphene can be manipulated by electrostatic and thermal control[113].

Resistance transduction is another transduction mechanism of graphene. Graphene has an exceedingly large surface-to-volume ratio, which enables electronic transport in graphene to be ultrasensitive to the surrounding chemical environment. Adsorption of molecules onto graphene results in the modulation of charge carriers by molecular or vicinity doping, which can be used for humidity and gas sensors[51,114,115]. The charge transfer by molecular adsorbates impacts the density of states of graphene at the Fermi level; therefore, graphene is capacitated to alter its conductivity[116,117]. Adsorbates behave as donors or acceptors depending on the doping abilities of the introduced molecules, thus resulting in a conductance change in graphene. Appropriate modification or functionalization results in drastic improvement in the sensitivity of graphene-based chemical sensors, and it can also provide guidance for better selectivity or specificity of graphene-based sensors[118].

Recently, a transduction mechanism based on the graphene-induced nonradiative transition for detecting MEMS force and acceleration was studied via analytical solutions and finite element analysis methods[119]. Specifically, the graphene-induced nonradiative transition is highly sensitive to distance, and the deflection of the graphene ribbon is highly susceptible to applied force or acceleration. In addition, a transduction mechanism based on the contact resistance of an improved graphene aerogel for detecting acceleration was reported in 2023[120].

Transfer methods for integrating graphene with target substrates

Graphene films can be derived from exfoliation, CVD synthesis, or epitaxial growth. The transfer of graphene works as a bridge connecting the production of graphene and its applications. To realize the applications of graphene in MEMS/NEMS, graphene typically needs to be transferred from the initial substrate to the target substrate. Concerning the graphene being transferred, having a clean surface and few defects on a large scale is crucial to the performance of graphene devices and is highly important for potential industrial applications of graphene films.

Transferring graphene prepared by mechanical exfoliation

Scotch tape[1] and the tip of an AFM silicon cantilever[121] are two earlier methods for mechanically exfoliating graphene flakes from a thin piece of graphite and simultaneously transferring the graphene flakes to the target substrate. Although mechanical exfoliation produces high-quality graphene flakes[122,123], their lateral size is normally limited to a few micrometers, and their thickness is not easily controlled.

Transferring graphene prepared via epitaxial growth

One of the methods used to produce large-scale and high-quality graphene sheets with a single orientation is epitaxial growth on SiC wafers by self-limiting sublimation of Si. Because the commonly used chemical etchants cannot dissolve SiC, traditional wet transfer methods cannot be used for transferring graphene grown on SiC substrates. Graphene grown on a SiC substrate can be transferred onto a target substrate via exfoliation or peeling techniques

according to the differential adhesion forces or binding energies between the graphene and different materials. For example, graphene can be transferred from a SiC substrate to a target substrate via either a bilayer film of gold (or palladium) or polyimide (PI), where the deposited metal layer provides the adhesion force and the PI works as a supporting layer during delamination[124,125], or a thermal release tape[126] or Scotch tape[127]. These methods usually cause issues, such as residues, defects, or unwanted doping of graphene. A water-soluble polymer poly(vinyl alcohol) (PVA) can be used to transfer graphene from a SiC substrate to a SiO_2/Si substrate with PVA dissolved in water; this method avoids the use of a chemical solvent, and thereby, doping-free graphene can be obtained[128]. In short, transferring graphene from a SiC to a target substrate is possible, but achieving high-quality transferred graphene is difficult, thus possibly hindering the widespread use of graphene in NEMSs. Therefore, methods for transferring graphene onto SiC should be further developed.

Transferring graphene prepared via CVD

CVD is an efficient method for synthesizing graphene on a large scale, and Cu is the most commonly used metal substrate for graphene grown by CVD because of the low C solubility of Cu, controllable number of graphene layers, and ease of transfer at a relatively low cost. Therefore, CVD graphene on a Cu substrate is used as an example to introduce transfer methods for graphene grown by CVD. A face-to-face transfer method for producing wafer-scale graphene films was developed by using nascent gas bubbles and capillary bridges between the graphene film and the underlying substrate during etching of the metal catalyst, thereby accomplishing both growth and transfer steps on one wafer (Fig. 4a)[129]. CVD graphene can be transferred via either wet or dry transfer, which are two basic methods.

Traditional wet polymer-supported transfer of CVD graphene

Among the wet transfer methods, which are an important way to transfer CVD graphene, polymer-supported transfer methods are the most used to transfer CVD graphene from the metal growth substrate to a target substrate. In most cases, PMMA is used as the polymer-supporting layer for wet methods for transferring CVD-grown graphene because of PMMA's relatively low viscosity, excellent wetting capability, flexibility, and good dissolubility in several organic solvents[130]. The typical transfer steps are basically as follows: first, the graphene on the back side of the growth substrate (e.g., Cu) is removed by O_2 plasma etching; second, the PMMA layer is spin-coated on the graphene and cured on a hotplate; third, the underlying Cu substrate is etched to free the PMMA/graphene layer; fourth, the PMMA/graphene is transferred to the target substrate; finally, the PMMA layer is dissolved in acetone and dried.

The etchants that are commonly used to remove the Cu substrate include aqueous solutions of iron nitrate, iron chloride, and ammonium persulfate. After the Cu substrate is removed, the metal particulates that can act as scattering centers to degrade the carrier transport properties are minimally removed by washing and normally require special cleaning technology[131]. However, cracks might easily form during the above graphene transfer because the surface of the Cu substrate is reconstructed at high temperatures during CVD growth and thereby becomes rough. The graphene is grown by following the rough surface of the underlying Cu substrate, and the graphene surface is also rough when the Cu is removed by the etchant. Because the rough surface of the graphene cannot be in full contact with the target substrate, gaps exist between them; consequently, cracks ultimately form during the dissolution of the PMMA layer[132]. To improve the contact between the graphene and the transfer target substrate and reduce the formation of cracks, a second layer of PMMA can be spin-coated after the PMMA/graphene stack is transferred to the target substrate[132]. In addition, some water probably remains in the gaps between the PMMA/graphene stack and the target substrate, thus leading to cracks after PMMA is removed. Therefore, it is helpful to improve the quality of the transferred graphene by baking the graphene samples (e.g., at 150 °C for 15 min) to evaporate the water between the graphene and the substrate before removing the PMMA (Fig. 4b)[131,133].

Based on the optimized wet PMMA-supported transfer method, a double-layer stacked graphene is created by transferring a monolayer CVD graphene to another monolayer CVD graphene on copper (Fig. 4c)[52,134]. The experimental results for this method confirmed that, for suspended structures made of monolayer CVD graphene, the addition of a second layer of CVD graphene disproportionally increases the fracture toughness of the resulting suspended graphene structure and indicated that suspended structures made of double-layer stacked CVD graphene have better overall mechanical resilience than do suspended structures made of monolayer CVD graphene[135–137].

PMMA is not typically removed entirely even after long exposures to acetone because of its high molecular weight and high viscosity, and the PMMA residues might cause charged impurity scattering and unintentional graphene doping[138], thereby affecting the graphene electrical properties, such as increased sheet resistance and related applications (such as in conductive electrodes)[132]. A thermal annealing step in a vacuum furnace under an H_2-Ar or H_2-N_2 environment is often used to remove as many PMMA residues as possible[139]. Notably, methods of

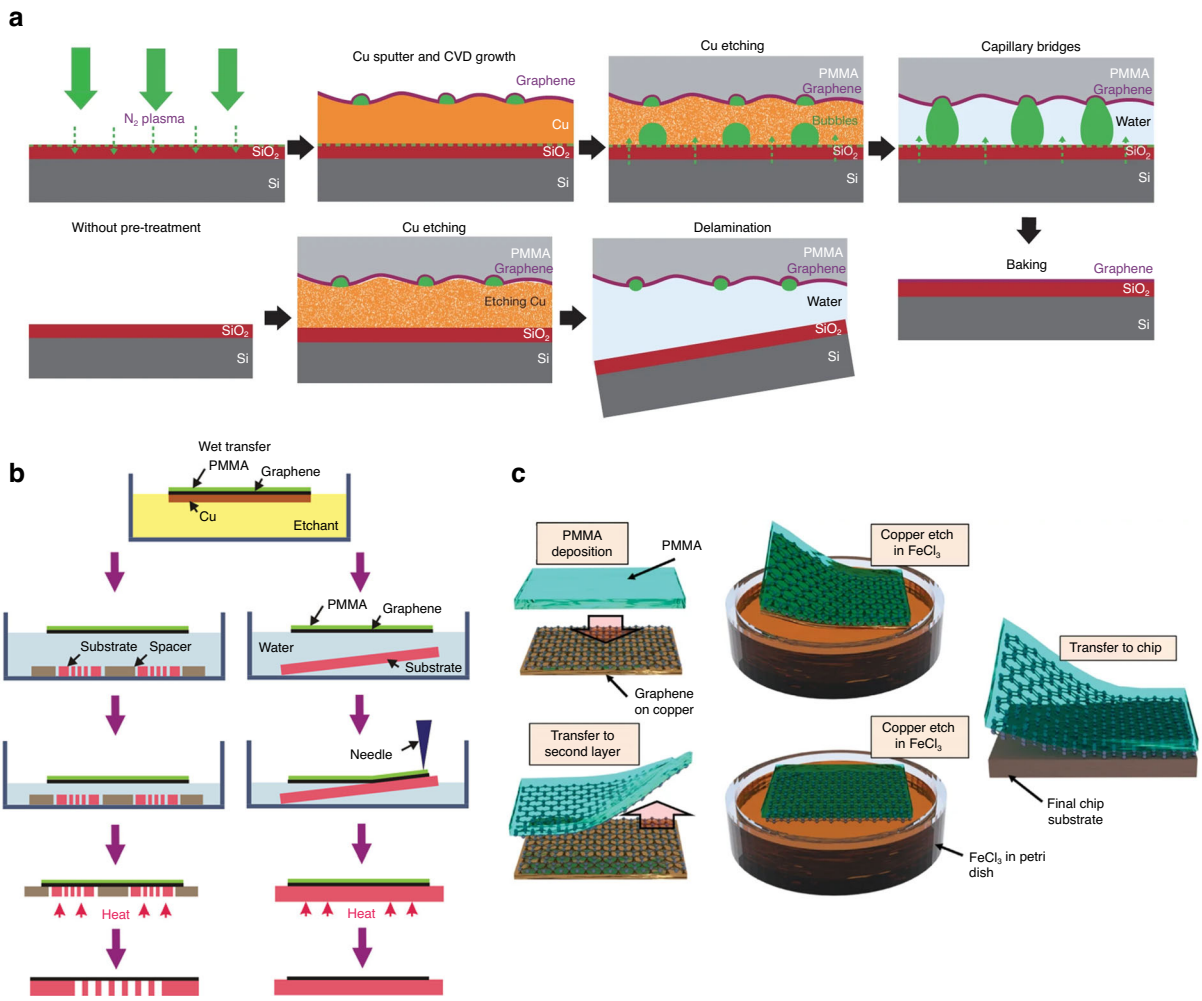

Fig. 4 Schematics of traditional wet polymer-supported transfer of CVD graphene. a A face-to-face method for transferring graphene via capillary bridges; the steps shown for this method are as follows: bubbling seeding via plasma treatment, CVD growth, Cu film etching, the formation of capillary bridges, and the removal of water and PMMA[129]. **b**, **c** Different methods of PMMA-based wet transfer of CVD-grown monolayer graphene[133,136]. Figures reproduced with permission from refs. [129,133,136]

annealing are unsuitable for flexible substrates because of the high temperature. There are also other improved methods for removing PMMA residues; these methods include inserting an organic small-molecule buffer layer with excellent solubility in the solvent between the graphene and the PMMA[140] or using UV irradiation to degrade the PMMA[141]. In addition to PMMA, poly(bisphenol A carbonate) (PC)[142], the polymer polyisobutylene (PIB)[143], pentacene ($C_{22}H_{14}$) (Fig. 5a)[144], anthracene[145], paraffin[146], photoresist[147], and rosin and/or anisole[148] are also used as supporting layers in wet transfer methods; these supporting layers might be helpful for obtaining clean, less doped and high-quality graphene.

Thermal release tape for wet transfer of CVD graphene

Many extended methods for transferring CVD graphene are based on basic polymer-supported transfer methods. For example, a thermal release tape can be used as an alternative to the polymers mentioned above and is often used to transfer graphene onto flexible substrates[149]. As shown in Fig. 5b, the thermal release tape method has been used to demonstrate roll-to-roll production of 30-inch graphene films for transparent electrodes[150]. A universal method for preparing large-area suspended mono- and few-layer graphene and other 2D materials was developed by using a thermal release tape to transfer graphene onto a densely patterned hole array substrate that is pretreated either with oxygen plasma or via gold film deposition (Fig. 5c)[151]. A method for achieving a clean and less defective transfer of monolayer graphene from copper foil onto the target substrate by floating the copper foil with the graphene in hot water and delaminating the graphene by using a thermal release tape has been reported[152].

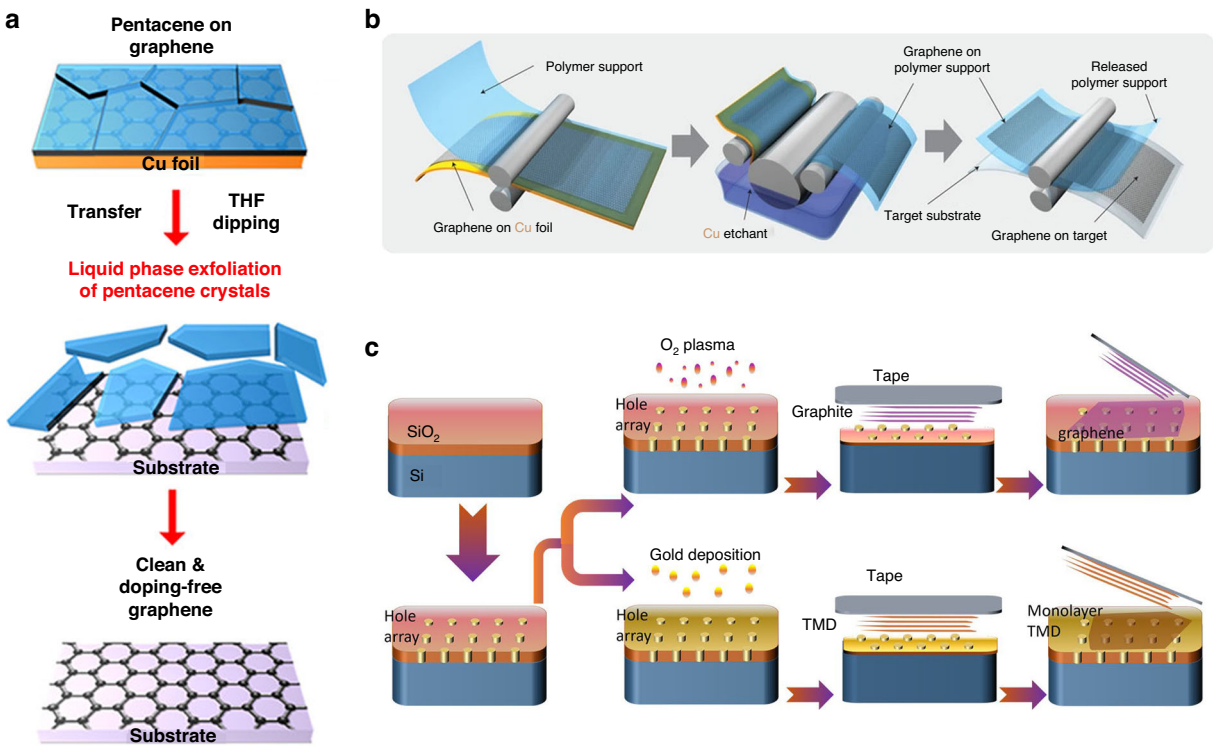

Fig. 5 Schematics of several typical methods for transferring CVD graphene. a A clean transfer procedure for transferring wafer-scale graphene from copper foil onto an arbitrary substrate by using pentacene as the supporting layer[144]. **b** A roll-to-roll transfer of 30-inch graphene films onto a copper foil[150]. **c** An efficient mechanical exfoliation method for transferring graphene and other 2D materials onto etched cavities[151]. Figures reproduced with permission from refs. [144,150,151]

Electrochemical delamination for the wet transfer of CVD graphene

Electrochemical delamination (also called "bubble transfer") is a fast transfer method for CVD graphene grown on a Cu substrate[153,154]. As shown in Fig. 6a, the fast delamination of graphene from the Cu substrate is induced by the production of hydrogen bubbles during the electrolysis of water. Electrochemical delamination can transfer graphene on both sides of metal substrates with high efficiency, and the metal substrates can be reused. In addition, electrochemical delamination can also be used to transfer graphene grown on chemical inserts or noble metal substrates, such as Ir, Pt, and Au; traditional wet graphene transfer methods cannot be used because of their low solubility and high cost. However, hydrogen bubbles produced during electrochemical delamination may lead to mechanical damage to the transferred graphene. Therefore, several other types of nondestructive electrochemical delamination methods without the production of bubbles have been developed[155,156].

Polymer-free methods for the wet transfer of CVD graphene

To avoid the polymer residues that are produced by polymer-supported transfer methods and improve the electrical properties (such as mobility) of transferred graphene, polymer-free methods[157] that transfer graphene without using a polymer-supporting layer have also been developed; examples of polymer-free methods include those that use a thin graphite holder (Fig. 6b)[158], a waterproof marker frame[159], or electrostatic force[160].

Dry transfer of CVD graphene

Dry transfer normally refers to transferring graphene onto the target substrate without using solutions. Similar to how PMMA is used as a polymer-supporting layer in wet transfer, PDMS and thermal release tape (Fig. 6c) are often used as polymer-supporting layers in dry transfer and can be removed by thermal treatment[43,161–164]. For example, the roll-to-roll method for transferring 30-inch graphene has been successfully developed[150]. Specifically, a thermal release tape was attached to graphene by two rollers, and then the Cu substrate was removed by the etchant. Next, the graphene was transferred to the target substrates via two rollers, and the thermal release tape was released by mild heating. The roll-to-roll method is suitable for transferring CVD graphene onto flexible target substrates on a large scale but easily causes mechanical defects when the CVD graphene is transferred to a rigid substrate. An improved roll-to-roll method involving the

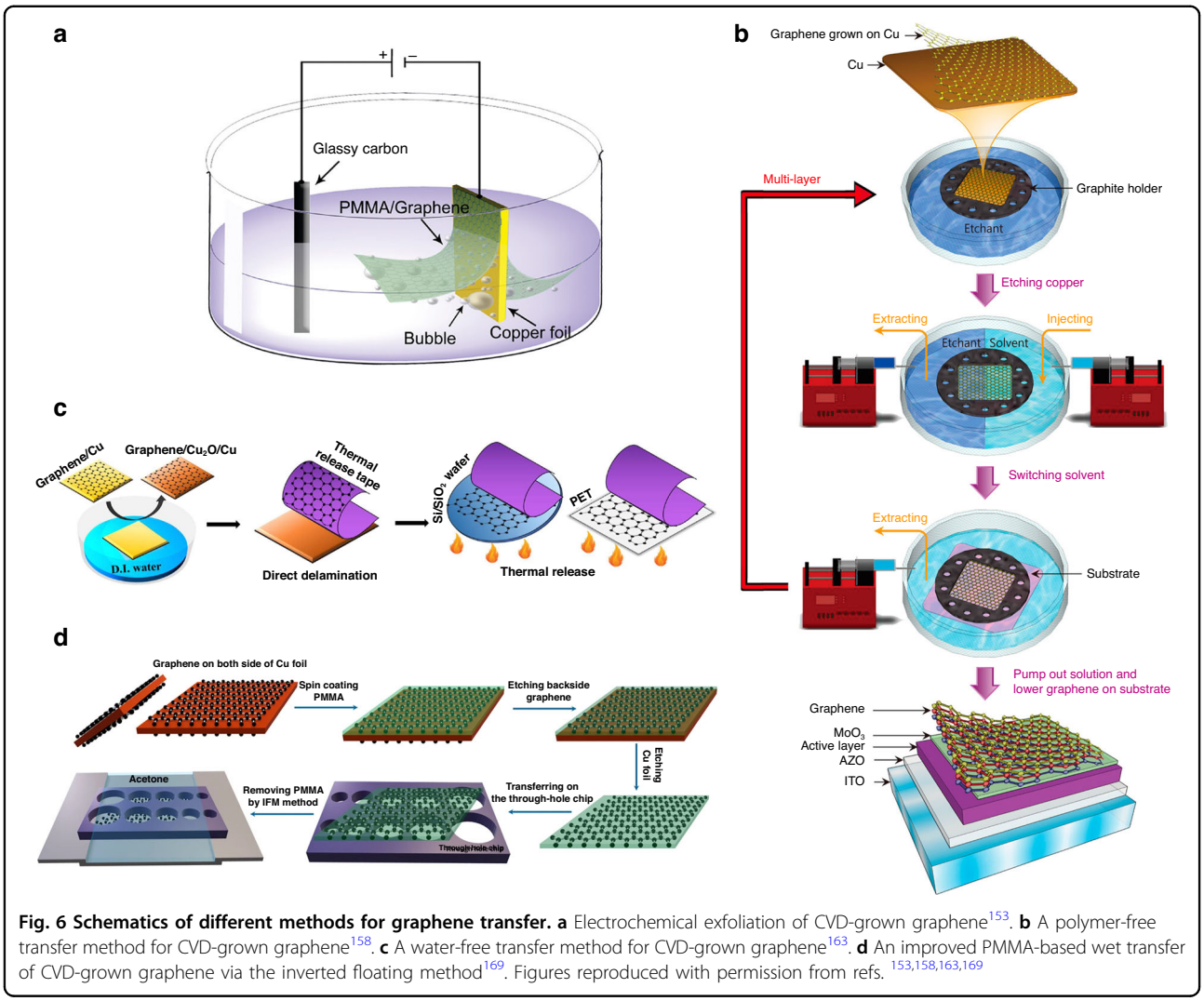

Fig. 6 Schematics of different methods for graphene transfer. a Electrochemical exfoliation of CVD-grown graphene[153]. **b** A polymer-free transfer method for CVD-grown graphene[158]. **c** A water-free transfer method for CVD-grown graphene[163]. **d** An improved PMMA-based wet transfer of CVD-grown graphene via the inverted floating method[169]. Figures reproduced with permission from refs. [153,158,163,169]

use of two hot pressure plates was developed[165]; in this method, CVD graphene can be transferred to either flexible or rigid substrates with relatively few defects. On the basis of differences in the adhesion of graphene to various metals, another improved roll-to-roll method involving the use of a thin metal film as the supporting layer of graphene and a thermal release tape was developed[166]; both sides of graphene on the Cu substrate can be transferred, and the Cu substrate can be reused. The dry-release transfer of monolayer and bilayer graphene by using poly(propylene) carbonate (PPC) films that have thermoplastic properties according to the adjustable temperature adhesion between the graphene and PPC was demonstrated[167]. Recently, a dry, sacrificial-layer-free, and scalable method for transferring graphene and other 2D materials and heterostructures via an adhesive matrix was reported; in this method, the low-adhesion substrate of interest is embedded in a matrix that promotes transfer through strong adhesive interactions with the 2D material[168]. In essence, to realize dry transfer, the adhesion energy between the graphene and substrate should be measured to precisely control delamination.

Other transfer methods for CVD graphene

Ultraclean monolayer and bilayer CVD graphene membranes up to 500 and 750 μm in size have been realized via the inverted floating method (Fig. 6d) followed by thermal annealing under vacuum[169], in which PMMA is used as the supporting layer. A generic methodology for the large-area transfer of graphene and other 2D materials via adhesive wafer bonding was developed[170]; this methodology avoids manual handling and is compatible with large-scale semiconductor manufacturing lines. A simple method of transferring large areas (up to A4-size sheets) of CVD graphene from copper foils onto a target substrate was developed by using a polyvinyl alcohol polymer and hot-roll office laminator[171]. Methods

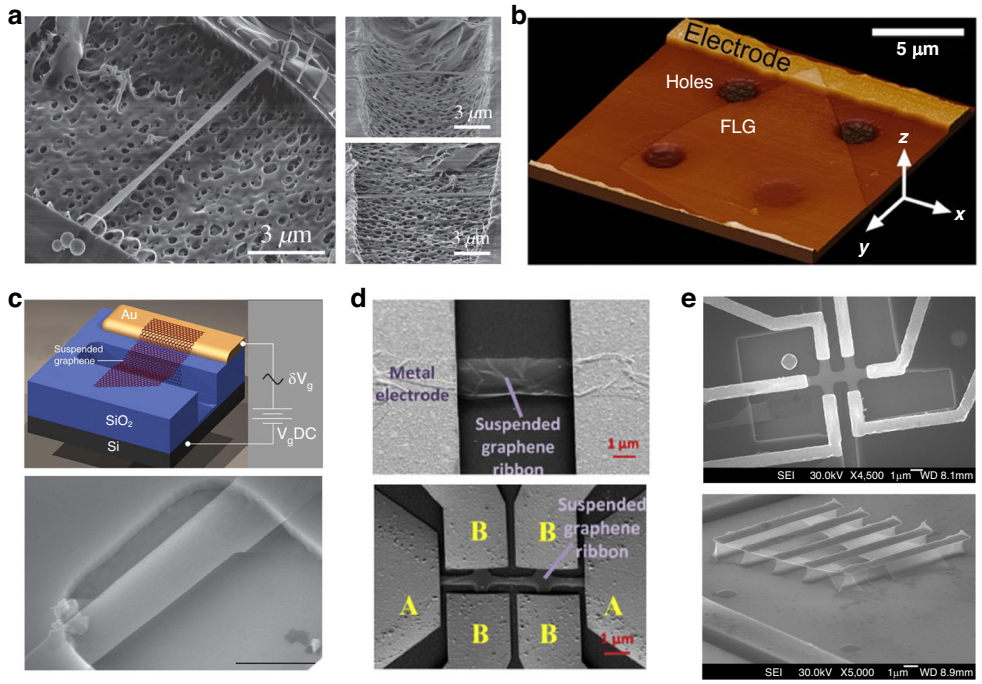

Fig. 7 Fabrication of suspended graphene structures. a A few-layer graphene suspended over an etched SU-8 trench for a high-quality factor NEMS resonator due to the thermal shrinkage of the SU-8-induced strain[180]. **b** An AFM topography image of freely suspended few-layer graphene connected to an electrode[178]. **c** Monolayer graphene suspended over an etched SiO_2 cavity for the NEMS resonator[14]. **d** SEM images of a graphene ribbon suspended between metal electrodes[182]. **e** SEM images of a high-mobility freely suspended graphene Hall bar that was fabricated on a polydimethylglutarimide-based organic polymer[181]. Figures reproduced with permission from refs. [14,178,180–182]

for the direct synthesis, etching, and transfer of large-scale and patterned graphene films have been developed[39].

Recently, several new graphene transfer methods have been developed. For example, facile transfer of graphene onto polyethylene without the use of a supporting layer was developed according to van der Waals interactions[172]. A general wafer-scale graphene transfer method based on gradient surface energy modulation was reported; this method results in reliable adhesion and a reliable release of graphene onto target substrate wafers[173]. The large-area transfer of 2D materials, including graphene, was developed by controllable conformal contact[174]; the transferred materials had the advantage of being free of cracks, contamination, and wrinkles. More approaches for transferring large-area graphene can be found in the previously reported literature[171,175–177].

As CVD graphene is transferred from its metallic growth substrate to a target substrate, the technology is compatible with semiconductor fabrication technology at the back end (BEOL). Nevertheless, unintentional contamination by water molecules, lithographic residues, and hydrocarbon contaminants during structuring and contact deposition can significantly influence the electronic system of graphene and modulate its charge carrier density. Notably, these contaminants remarkably limit the sensitivity and applicability of graphene-based sensors.

Fabrication of suspended graphene structures

Generally, to fabricate graphene NEMS structures, realizing freely suspended graphene (membranes, beams, or ribbons) is typically required (Fig. 7a–e)[18,178,179]. Depending on the methods of graphene synthesis, such as CVD on metal foils, mechanical/liquid phase/thermal exfoliation, chemical reduction of graphene oxide, and epitaxial graphene on SiC, three main approaches to fabricating suspended graphene include direct mechanical exfoliation of pristine graphene onto prepatterned substrates with trenches or cavities, etching of the substrates underneath the graphene in a final processing step via HF-based wet or dry etching, and transferring CVD-grown graphene directly onto prepatterned substrates with trenches or cavities.

Early suspended graphene sheets were produced by mechanical exfoliation, which restricted scalable fabrication and standardized processes. CVD-grown graphene is a good candidate for fabricating suspended graphene sheets on a large scale via a standardized lithography process. When a wet etching process, such as liquid HF etching, is employed to release the graphene, special care must be taken to avoid the collapse of the suspended graphene by capillary forces and to avoid peeling off the electrodes. The common methods to avoid such collapse are to employ buffered hydrofluoric (BHF) etching followed by critical point drying (CPD) or

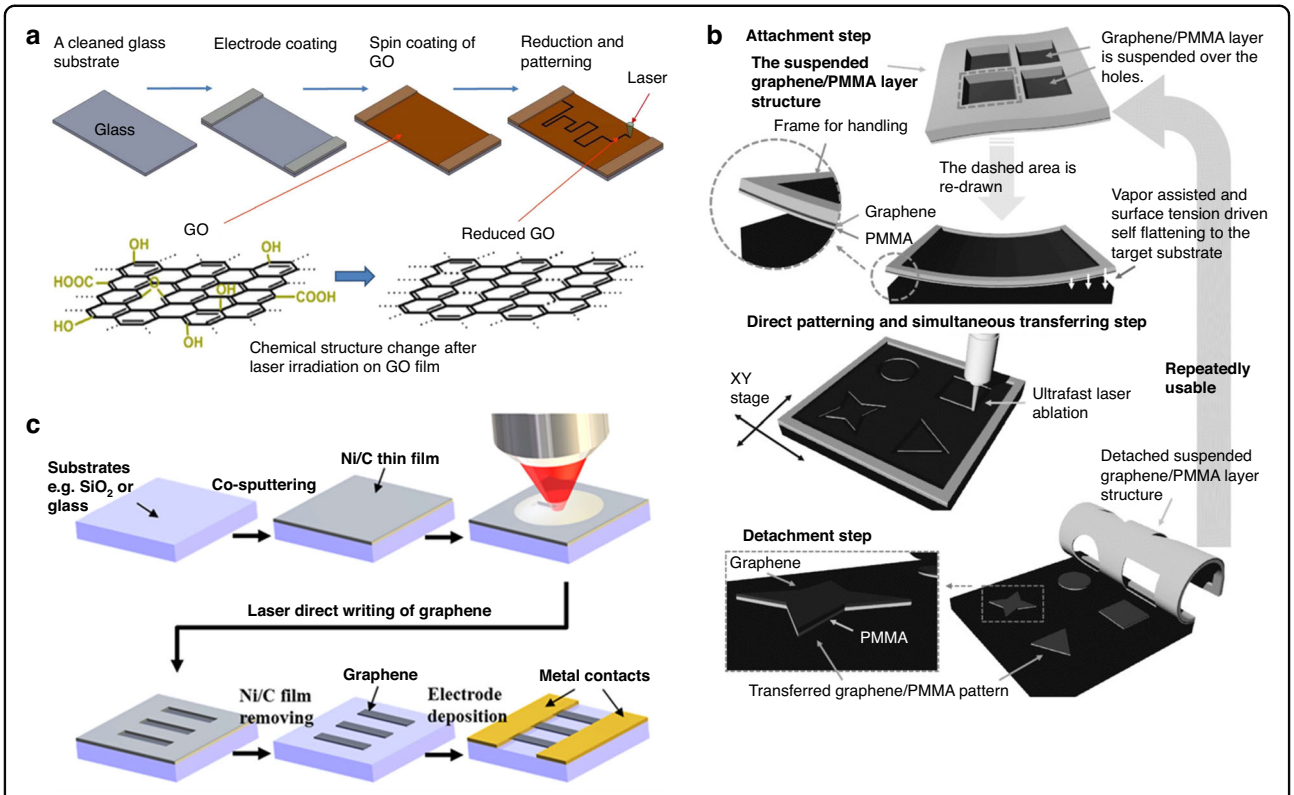

Fig. 8 Patterning of graphene. a Laser direct patterning of a reduced-graphene oxide[186]. **b** Laser-induced direct graphene patterning and simultaneous graphene transfer[187]. **c** A laser direct writing process to pattern graphene on insulating substrates under ambient conditions[189]. Figures reproduced with permission from refs. [186,187,189]

to employ HF vapor. However, the realization of suspended graphene via HF-based etching also has several drawbacks; for example, HFs, especially liquid BHFs, easily attack Ti, which is often used as a metal electrode material for Ohmic contact with graphene. In addition, the SiO_2 underneath the metal electrodes is also easily etched to some extent due to the isotropic etching of BHF, which might affect the stability of the mechanical structures. Thus, finding alternative ways to replace HF etching-based methods to realize suspended graphene structures is meaningful. There are several methods for suspending graphene on organic polymer substrates by using e-beam lithography-based processes to remove parts of the sacrificial polymer layer, thereby avoiding the use of aggressive BHF etching processes (Fig. 7a, e)[87,180,181]. In the fabrication process of suspended graphene devices, more attention needs to be paid to cleaning because traditional cleaning methods, such as ultrasonic-assisted dissolution or oxygen ashing, are too aggressive for graphene[182].

Patterning and electrical contact of graphene

Patterning of graphene

Typically, graphene must be patterned after it is transferred from the initial substrate to a target substrate for device applications. Although graphene is intrinsically nanoscale, it can be patterned at the wafer scale by a standard lithographic process and O_2 plasma etching, which is the most commonly used method for patterning graphene, where a hard or a resist mask is employed[135,183]. For patterning the graphene flakes derived from mechanical exfoliation, standard optical lithography is unavailable, but e-beam lithography or shadow masks are alternative methods. Recently, there have also been reports associated with the laser patterning of graphene after transfer (Fig. 8a, b)[184–187] and laser direct writing of graphene patterns on target substrates (Fig. 8c)[188,189]. The method for patterning graphene via a laser is flexible and can avoid the possible contamination from photoresist, which the standard lithography process requires. Nanoscale patterning of graphene is also achieved via various methods, such as femtosecond laser ablation[190], local catalytic etching via atomic force microscopy equipped with an Ag-coated probe[191], and focused ion beams, such as helium ion beams[192]. In addition, patterned graphene films can also be directly grown on patterned metal growth substrates (such as Ni layers via CVD) and then transferred to target substrates (such as SiO_2 substrates) without additional lithography processes[43].

Electrical contact of graphene

Like patterning, graphene must be electrically contacted after the graphene is transferred from the initial substrate to a target substrate for device applications. The metal electrodes for electrically contacting graphene can be fabricated by thermal evaporation or sputtering either before or after graphene transfer. As shown in previous reports[50–53,135,183] on graphene-based devices, such as humidity and gas sensors, pressure sensors, and accelerometers, before graphene is transferred to a prefabricated SiO_2/Si substrate, a 50 nm thick layer of Ti followed by a 270 nm thick layer of Au is evaporated into the pre-etched cavities of the SiO_2 layer, thus leaving the patterned Au electrodes to protrude ~20 nm above the SiO_2 surface (Fig. 9a)[53]. One of the advantages of fabricating contact electrodes before graphene transfer is that the cleanliness of the graphene surfaces is improved, and the risk of rupturing the graphene membranes during processing is reduced. Additionally, the graphene–metal contacts are not easily degraded by polymer residues in this way. For a chip package, gold wires are normally bonded from the package to the metal contact pads. The contact resistance between graphene and metal electrodes is crucial for high-performance graphene devices. One review of the literature[193] is specifically associated with studies on the graphene–metal contact characteristics in terms of the metal preparation method, asymmetric conductance, annealing effect, and interface impact. There are also two review studies[194,195] related to electrical contact with one- and two-dimensional nanomaterials. As shown in Fig. 9b–e [196–199], the contact resistance of graphene devices can be improved by edge-contacted metal–graphene interfaces, the theoretical and experimental study of which has been reported[196–200]. For example, enhanced carrier injection is experimentally achieved in graphene devices by forming cuts in the graphene within the contact regions. These cuts are oriented normally to the channel and facilitate bonding between the contact metal and carbon atoms at the graphene cut edges, thereby reproducibly maximizing "edge-contacted" injection[199].

NEMS devices based on suspended graphene

The earliest study on suspended graphene membranes for NEMS applications in 2007 involved doubly clamped electromechanical resonators that were made of mechanically exfoliated graphene flakes suspended over trenches with thicknesses ranging from monolayer to multiple layers[14]. The fabricated devices represent the thinnest mechanical resonators ever produced and can be actuated by optical or electrical methods in the megahertz range. Following this initial breakthrough, various types of NEMS resonators based on doubly clamped suspended graphene beams and fully clamped suspended graphene membranes have been developed; these resonators include graphene NEMS resonators that can sense mass and temperature[201]. In 2013, the first graphene NEMS pressure sensor with high sensitivity, a small footprint, and electrical readout capabilities was realized by suspending a monolayer CVD graphene membrane over the etched cavity[34]. Current applications of suspended graphene in NEMSs have extended from resonators[202,203] and pressure sensors[34] to other types of NEMS devices[23,204], such as strain sensors[205], nanoelectromechanical switches[93], earphones[206], microphones[95], loudspeakers[94], accelerometers[135,183], and bolometers[207–209]. In this section, we discuss the applications of suspended graphene membranes, beams, and ribbons in various types of nanoelectromechanical devices.

Piezoresistive pressure sensors

As shown in Fig. 10a, b, graphene pressure sensors based on the piezoresistive effect have been widely reported[34,70,210,211]. Piezoresistive pressure sensors based on suspended graphene membranes with ~20 to 100 times higher sensitivity per unit area (this sensitivity is greater than that of conventional piezoresistive pressure sensors, have been demonstrated[34,70]. In addition, by employing the intrinsic piezoresistivity of graphene to transduce its motion, a suspended H-shaped monolayer graphene resonator clamped at the base by four gold electrodes, and SiO_2 was fabricated by underetching SiO_2 via buffered hydrofluoric acid and critical point drying; this resonator can be used for sensing mass and force with high sensitivity (Fig. 10c)[212]. Piezoresistive graphene pressure sensors normally require the impermeability of suspended graphene membranes over cavities. One of the challenges in bringing these sensors into volume production is realizing a hermetically sealed cavity with a reference pressure that remains constant for several years. Although it has been claimed that graphene is impermeable[30], the leakage rates of graphene-sealed cavities are relatively high compared with those of commercial pressure sensor cavities. In addition, obtaining piezoresistive graphene pressure sensors is challenging because of the defects, such as holes and cracks, in suspended graphene membranes.

In addition to pressure sensors based on self-suspended graphene, several pressure sensors use partly suspended graphene with polymers or other membranes[59,213,214]. For example, by transferring few-layer CVD-grown graphene onto a suspended silicon nitride thin membrane that was perforated by a period array of micro through-holes, graphene-based pressure sensors were realized with a sensitivity of 2.8×10^{-5} $mbar^{-1}$ and good linearity over a wide pressure range[59]. Another piezoresistive pressure sensor based on multilayer CVD graphene meander

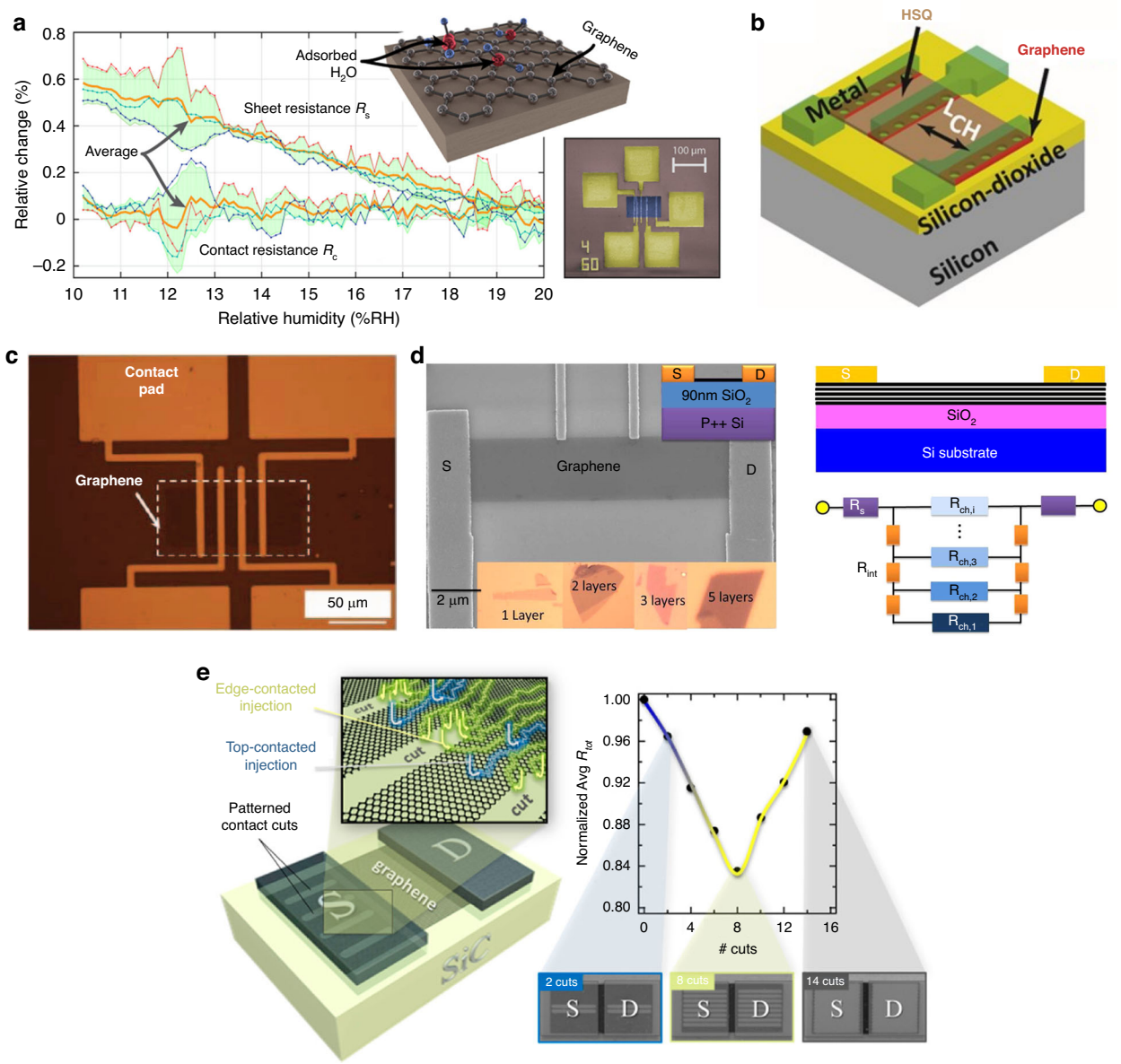

Fig. 9 Electrical contact of graphene. a Gold–graphene contact resistance and sheet resistance of graphene versus relative humidity[53]. **b** The graphene under the electrodes was intentionally etched to create holes of different sizes to reduce the contact resistance[196]. **c** Structures used for measuring metal–graphene contact resistances[197]. **d** An SEM image of a four-terminal few-layer graphene device that was used to study the electrical impact of edge contacts and a resistor network model of conventional top-contacted few-layer graphene[198]. **e** A two-terminal graphene device with cuts patterned perpendicular to the channel in the contact region; these cuts can reduce contact resistance[199]. Figures reproduced with permission from refs. [53,196–199]

patterns located on the maximum strain area of a suspended 100 nm thick, 280 μm wide square silicon nitride membrane was reported[61].

Capacitive pressure sensors

Graphene-based capacitive pressure sensors have been reported (Fig. 11a–d)[77,213,215–217]. For example, ultra-large suspended graphene membranes with few-layer graphene over a circular hole with a diameter of up to 1.5 mm on a quartz substrate were realized via a hydrogen bubbling transfer approach with thermal annealing; these graphene membranes were used for capacitive pressure sensors in an impermeable chamber; the results revealed a linear response and a high sensitivity of 15.15 aF Pa^{-1}, which is 770% greater than the sensitivity of conventional silicon-based membranes[77].

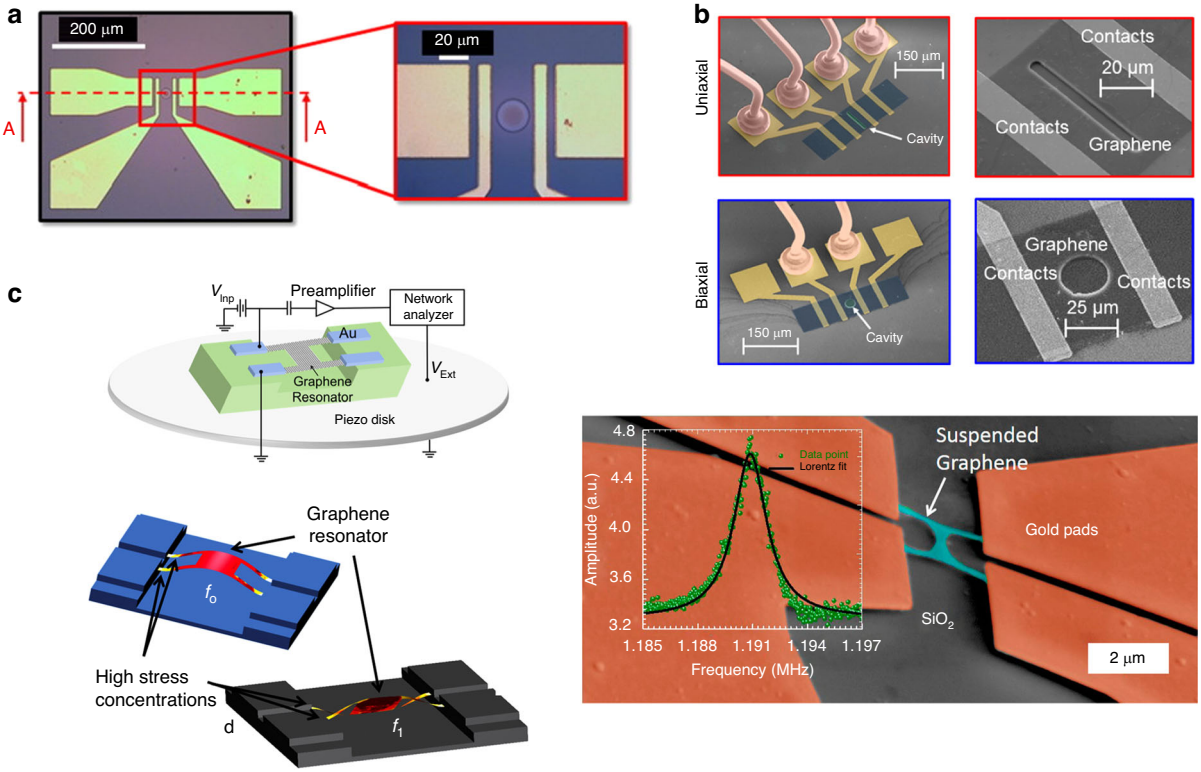

Fig. 10 Piezoresistive pressure sensors and transducers. a An optical micrograph of a suspended graphene membrane-based piezoresistive NEMS pressure sensor[210]. **b** SEM images of piezoresistive NEMS pressure sensors based on monolayer graphene suspended over an etched rectangular SiO_2 cavity and an etched circular SiO_2 cavity[70]. **c** Ultrasensitive room-temperature piezoresistive transduction in a graphene NEMS. This figure part shows a circuit diagram of the measurement setup, a finite element model, and an SEM image of a fabricated suspended H-shaped graphene resonator[212]. Figures reproduced with permission from refs. [70,210,212]

Another capacitive pressure sensor fabricated on top of an insulating quartz substrate consisted of circular AuPd bottom and AuPd top electrodes that were separated from the bottom electrode by a spin-on-glass dielectric layer, and a few-layer graphene membrane was suspended over the sealed cavity of the AuPd top electrode[215]. The capacitance changes of a graphene drum as low as 50 aF and pressure differences as low as 25 mbar were successfully measured.

In addition to capacitive pressure sensors based on self-suspended graphene, capacitive pressure sensors have been realized by using a suspended ultrathin CVD-grown graphene/PMMA heterostructure membrane over a large array of microcavities, each up to 30 μm in diameter, thus showing reproducible pressure transduction under static and dynamic loading up to pressures of 250 kPa and pressure sensitivity of 123 aF Pa^{-1} mm^{-2} over a pressure range of 0–100 kPa[213,214].

Resonant pressure and mass sensors

Graphene pressure sensors based on the resonance effect have been developed[96,218–220]. For example, squeeze-film pressure sensors are based on the pressure dependence of the membrane frequency; this pressure dependence is caused by the compression of the surrounding gas, thereby changing the stiffness of the resonator, which normally requires strong, flexible, and light membranes. As shown in Fig. 12a, via a laser interferometry setup for detecting the resonance frequency of the graphene drum, pressure sensors using a few-layer graphene membrane as a squeeze film to cover a gas cavity were demonstrated to have a frequency shift of 4 MHz between 8 and 1000 mbar and a sensitivity of 9000 Hz/mbar; although these results were 45 times greater than that of state-of-the-art MEMS-based squeeze-film pressure sensors, the pressure sensors shown in Fig. 12a used a 25-fold smaller membrane area[96]. In addition, Fig. 12b shows that resonant pressure sensors using suspended multilayer exfoliated graphene flakes as a sealed drum with low tension were fabricated on insulating sapphire substrates with a local back gate that was used to directly actuate radio frequencies actuation and detect the mechanical resonance modes, thus resulting in high gate tenability (~1 MHz/V) of the resonator modes[219]. In these resonant sensors, the shifts in the resonator mode frequency with the force exerted by

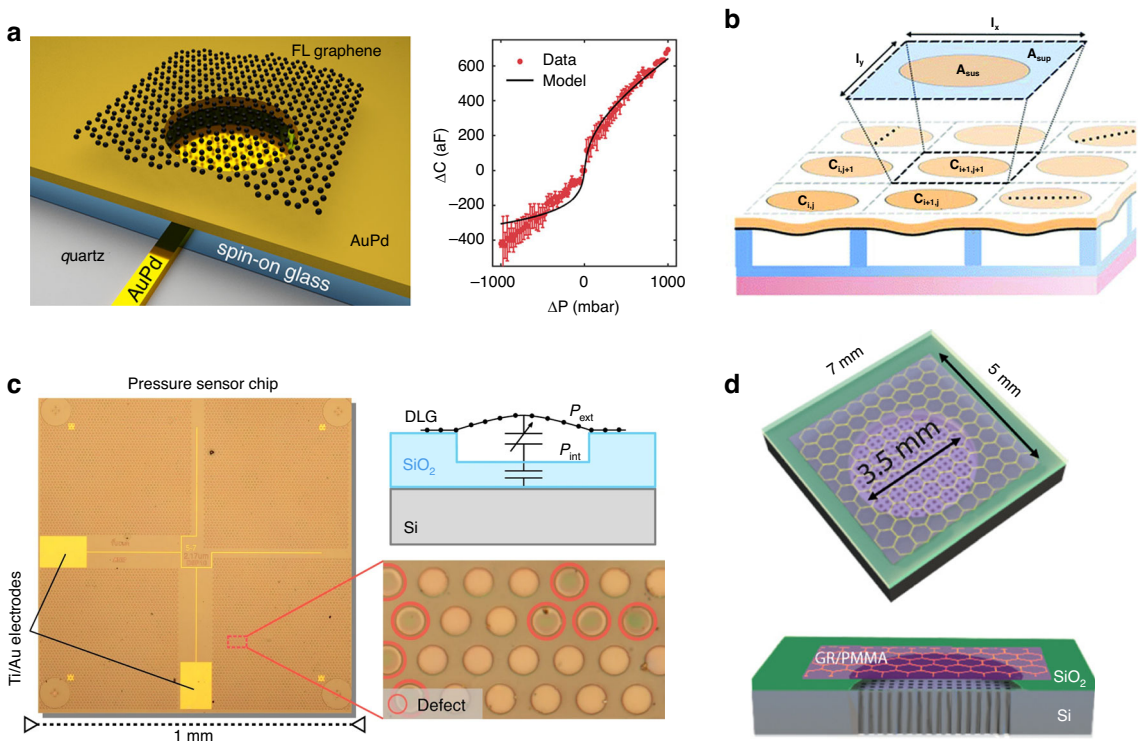

Fig. 11 Capacitive pressure sensors based on suspended graphene. a A static capacitive pressure sensor using a single graphene drum[215]. **b** A schematic of a capacitive pressure sensor array using suspended graphene–polymer heterostructure membranes[213]. **c** Sensitive capacitive pressure sensors based on suspended double-layer graphene/PMMA membrane arrays[216]. **d** A schematic of a suspended graphene/PMMA acoustic capacitive sensor created by etching the SiO_2 sacrificial layer[217]. Figures reproduced with permission from refs. [213,215–217]

the helium gas molecules above the membrane were studied, and the sensing capability of 1 Torr pressure was demonstrated in a cryogenic environment[219].

The equation of the resonance frequency $f = \frac{1}{2\pi}\sqrt{\frac{k}{m}}$ shows that a small mass change[221–223] Δm causes a large frequency shift $\Delta f = -\frac{\Delta m}{2m} f$ because of the high resonance frequency f and low mass m of graphene membranes. Therefore, suspended graphene membranes can be very suitable for mass sensing[201,224]. One of the challenges of mass sensors based on suspended graphene membranes is that the detected shift in resonance frequency is determined by both the mass and position of the mass[225]. The mass of a particle can be determined independently of position by analyzing the frequency shift of multiple well-characterized vibrational modes[226].

Nanoelectromechanical switches

Nanoelectromechanical switches can help reduce power consumption, but reliable nanoelectromechanical switches with low operating voltages and low contact resistances are still challenging and easily fail because of irreversible switching or stiction. Nanoelectromechanical switches employing suspended graphene as movable elements have been developed because of their high Young's modulus, extremely low mass, and outstanding carrier mobility and are divided into 2-terminal and 3-terminal NEMS switches[83–87,89,91–93,227]. The on and off states of the switches are normally controlled by modulating the electrostatic force applied to graphene. A 2-terminal switch operates by deflecting a suspended graphene membrane with a source-drain voltage and measuring the current once contact. A 3-terminal NEMS switch uses third electrodes to apply an actuation voltage independent of the source-drain voltage and provides merits such as greater operational flexibility, lower power consumption, and a higher level of integration.

An early electromechanical switch with two CVD-grown graphene electrodes was realized; this switch could switch several times at a low operation voltage (~4.5 V) until the top graphene beam remained in permanent electrical contact with the bottom graphene film[83]. A low pull-in voltage of 1.85 V and a very fast estimated switching time of 40 ns were realized in NEMS switches based on a doubly clamped suspended few-layer graphene beam with a 150 nm air gap[84]. A low pull-in voltage of less than 2 V in graphene NEMS switches based on a simple bottom-up procedure using a polymer sacrificial spacer rather than acid etching was also realized[87]. In addition,

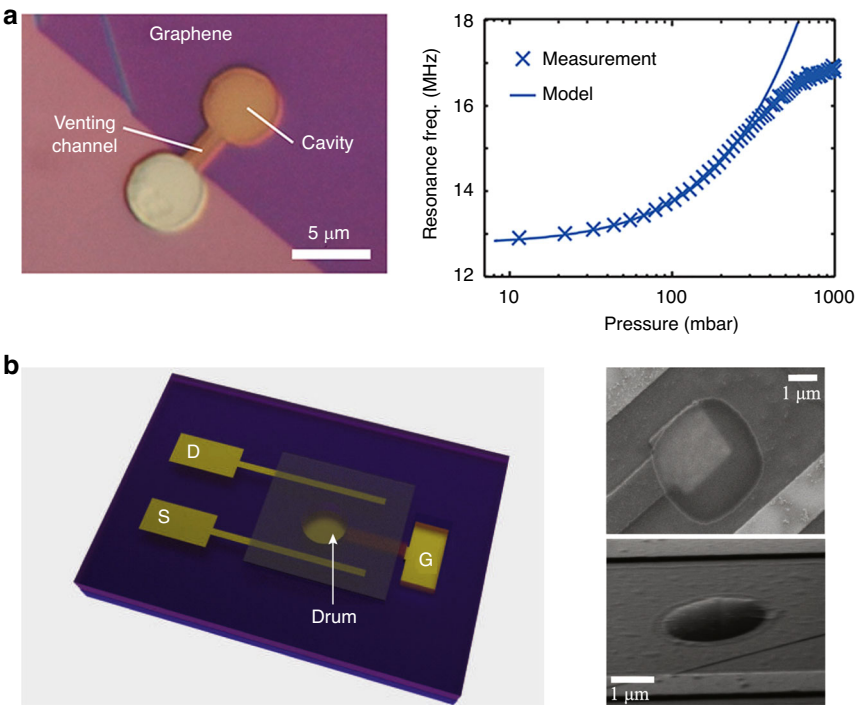

Fig. 12 Resonant pressure sensors based on suspended graphene. a A graphene squeeze-film pressure sensor[96]. **b** Graphene drums with low tension for electromechanical resonant pressure sensing[219]. Figures reproduced with permission from refs. [96,219]

an electromechanical thermal switch based on flexible, collapsible graphene membranes with a low operating voltage of ~2 V and a thermal switching ratio of ~1.3 was reported in 2021[228].

Most of the abovementioned graphene NEMS switches are based on doubly clamped beams and commonly suffer reliability problems because of tears on open edges and/or irreversible stiction of the graphene. To avoid the occurrence of tears in the graphene and to limit stiction, a large array of circularly clamped graphene NEMS switches with a unique design and sub5 V actuation voltage were fabricated via a bottom-up process[91]. They work with either 2-terminal or 3-terminal switching and have line contact during switching to reduce the contact area, thereby holding the potential to address the stiction challenges[91]. Compared with the structures of two-end fixed beams, the structures of cantilevers might have better linear behavior and high sensitivity. Both two-terminal and three-terminal NEMS switches based on suspended graphene cantilever beams were demonstrated with pull-in voltages ranging from 5 to 10 V[89]. In addition, nanocrystalline graphene directly deposited on insulating substrates can also be used for fabricating high-performance NEMS switches with top electrode contacts on a large scale; these switches exhibit a low pull-in voltage below 3 V, reversible operation, a minimal leakage current of 1 pA, and a high on/off ratio of 10^5 [93]. A high on/off ratio of 10^5 was also realized in a graphene NEMS switch with high reproducibility on the basis of locally defined nanomembrane structures in the graphene films on a SiC substrate with atomic steps[85].

Microphones and loudspeakers

In addition to being used for graphene electrostatic switches, graphene is used for electrostatic loudspeakers and microphones[94,95,229–231]. Graphene is electrically conductive, has an extremely small mass density, has a high mechanical strength and can construct mechanical resonators, all of these characteristics make graphene an excellent building material for small, efficient, high-quality broadband electrostatic audio speakers[145,217,229,230,232–238]. On the one hand, the low mass of graphene due to its atomic thickness ensures the high-frequency response of electrostatic audio speakers. On the other hand, the exceptional mechanical strength of graphene allows for relatively large and thin suspended diaphragms, thus reducing the effective spring constant that is required for an effective low-frequency response from electrostatic audio speakers.

A robust speaker built from a multilayered graphene diagram has an excellent frequency response across the entire audio frequency range (20 Hz–20 kHz), with performance matching or surpassing that of commercially

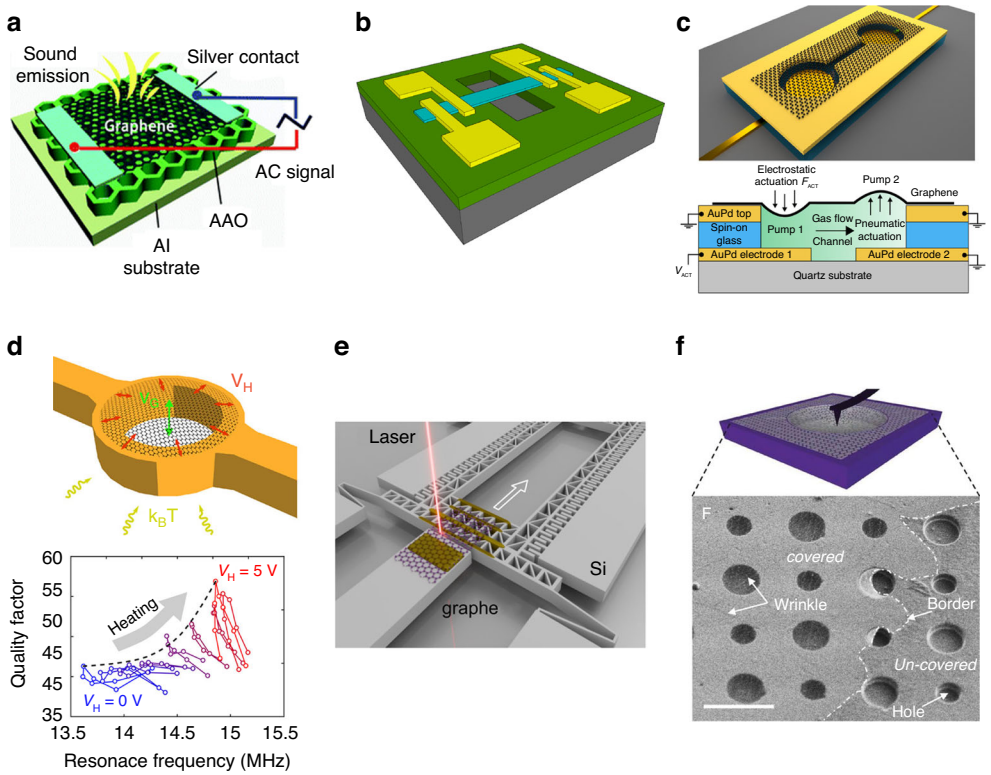

Fig. 13 NEMS devices based on suspended graphene and characterization of suspended graphene in NEMS structures. a A schematic view of a monolayer graphene sound-emitting device using anodic aluminum oxide (AAO) templates as substrates[241]. **b** A schematic of a Pirani pressure sensor, in which multilayer graphene suspended over a SiO_2 cavity is the sensing element[242]. **c** Graphene gas pumps[244]. **d** On-chip heaters for the tension tuning of graphene nanodrums[256]. **e** A schematic of a comb-drive (CD) actuator that applies uniaxial strain to a graphene flake by moving[257]. **f** AFM nanoindentation experiment of suspended graphene over cavities for measuring Young's modulus[259]. Figures reproduced with permission from refs. [241,242,244,256,257,259]

available audio earphones[94,95]. Multilayer graphene was used as a membrane material for condenser microphones; with a greater than 10 dB increase in sensitivity, these microphones outperform high-end commercial nickel-based microphones over a significant part of the audio spectrum[229]. A highly sensitive microphone for a hearing aid using a graphene-PMMA laminated diaphragm was created[239]. The graphene-based thermoacoustic loudspeakers[240,241] are especially effective in the ultrasonic frequency region because of the small heat capacity of graphene, in which graphene works as a stationary heater to heat the surrounding air, thereby generating time-dependent pressure vibrations, such as sound waves via thermal expansion (Fig. 13a).

Other NEMS devices based on suspended graphene without an attached mass

Suspended graphene can also be used in other aspects of NEMS. For example, a Pirani pressure sensor based on a multilayer suspended graphene strip was realized; the sensor featured a substantially decreased footprint and lower power consumption (Fig. 13b)[242]. A noninvasive local optical probe system consisting of a multilayer graphene resonator that is clamped to a gold film on an oxidized silicon surface can be used for quantitatively measuring motion and stress within a NEMS, based on Fizeau interferometry and Raman spectroscopy[90]. A suspended graphene membrane-based gas osmometer with a responsivity of 60 kHz $mbar^{-1}$ was demonstrated on the basis of osmotic pressure-induced deformation of graphene membranes that separate two gases at identical pressures[243]. The osmotic pressure was caused by differences in the rates of gas permeation into a cavity enclosed by few-layer graphene, and the deflection of the membrane was measured on the basis of the tension-induced resonance frequency via a laser interferometric technique[243]. Likewise, as shown in Fig. 13c, via the laser interferometric technique, a proof-of-principle for using suspended graphene membranes to pump attolitre quantities of gases at the nanoscale was demonstrated by measuring the deformation of each thin few-layer graphene drum suspended over two circular cavities connected by a narrow trench[244]. Both the cavities and the trench were covered by the graphene membrane, and the

local electrodes at the bottom of each cavity allowed each membrane to deform separately on the basis of electrostatic forces and allowed gas to flow inside the trench.

Recently, room-temperature detection of the individual physisorption of CO_2 molecules with suspended bilayer graphene was reported[245]; a unique device was designed to induce tensile strain in the bilayer graphene to prevent its mechanical deflection onto the substrate by electrostatic force. In 2022, bilayer graphene drums were used to measure the nanomotion of single bacteria in aqueous growth environments[246]. In 2023, NEMS temperature sensors based on suspended graphene were realized on the basis of the piezoresistive properties of graphene[247].

Characterization of the suspended graphene in the NEMS structures

NEMS structures can also be used for investigating the properties of graphene[248–255], such as Young's modulus, tension, and strain. An on-chip heater platform for locally tuning the in-plane tension of few-layer graphene nanodrums and investigating the origin of dissipation was reported (Fig. 14d)[256]. The thermomechanical resonance frequency and quality factor of graphene can be tuned by increasing the in-plane tension caused by Joule heating of the underlying metallic suspension ring[256]. To avoid any spurious effects due to capacitive coupling to the suspended graphene flake or interaction with the substrate for strain engineering, silicon micromachined comb-drive actuators were fabricated to controllably and reproducibly induce strain in a suspended graphene sheet entirely mechanically (Fig. 14e)[257]. In addition, the optimized comb-drive actuator can also be used for strain-dependent transport measurements of suspended graphene[258]. Suspended graphene structures can be used for measuring the Young's modulus of graphene (Fig. 14f)[5,33,259–262].

The importance of studying the permeability of suspended graphene in NEMSs lies in their ability to understand the transport mechanisms and interactions of materials at the atomic level and to facilitate the development of new efficient and selective permeable materials. Monolayer graphene with grain boundaries or line defects selectively allows small molecules of gases to pass through. However, large-molecule gases, such as oxygen and nitrogen, can hardly pass through the lattice gaps of graphene[263]. Many advanced methods, such as chemical treatment[264–266], thermal treatment[267], and interlayer modulation[268], have been performed on graphene to modify its permeability. More recently, studies have been conducted to increase the permeability of graphene by introducing nanopores[269]. As a result, the prepared suspended monolayer graphene gas-phase transport molecular valves with discrete angstrom-level pores enable precise control of gas permeability[269].

Accelerometers based on suspended graphene with an attached mass

As discussed above, doubly clamped graphene beams, fully clamped graphene membranes, and graphene cantilever beams for applications such as resonators, pressure sensors, switches, and loudspeakers/microphones have been widely studied. However, there are few reports on suspended graphene with attached masses. The limited number of such examples includes micrometer-sized few-layer graphene cantilevers with diamond allotrope carbon weights fabricated by using focused ion beam (FIB) deposition for studying the mechanical properties of graphene (Fig. 14a)[270], a kirigami pyramid and cantilevers made of suspended graphene supporting 50-nm-thick gold masses that were kept in a liquid to maintain their mechanical integrity (Fig. 14b)[271], and a suspended graphene membrane circularly clamped by SU-8 supporting an additional mass made of either SU-8 or gold located at the center of the graphene membrane for shock detection from ultrahigh mechanical impacts (Fig. 14c)[272]. All these previous reports involve extremely small masses, and the employed fabrication methods, such as FIB-induced deposition, are slow and typically incompatible with large-scale manufacturing.

Recently, the structures of both suspended graphene membranes and ribbons with large attached SiO_2/Si proof masses were realized via a robust, scalable, and high-yield MEMS manufacturing approach, and their potential applications in sensitive NEMS piezoresistive accelerometers were demonstrated (Fig. 14d, e)[135,183]. The die areas of such graphene-based NEMS accelerometers are at least two orders of magnitude smaller than those of conventional state-of-the-art silicon accelerometers[135,183]. Ultrasmall and combined spring-mass and piezoresistive transducers based on suspended graphene with an attached mass[135,136,183,273–276] are expected to pave the way for a new class of graphene NEMS devices, such as accelerometers with decreased size but increased performance.

Devices based on nonsuspended graphene

Flexible transparent conductive electrodes

In addition to the applications of suspended graphene in NEMS, the combination of graphene with conventional membranes also has wide applications in MEMS/NEMS. Owing to their excellent optical transmittance, electrical conductivity, stretchability and mechanical strength, graphene films can be integrated with soft substrates (such as polyethylene terephthalate (PET), PDMS, or PET coated with a PDMS layer[43,132,150]) as large-scale stretchable and foldable transparent conductive electrodes for flexible and wearable device applications (including high-speed field-effect transistors, touch screens, flat panel displays, light-emitting diodes

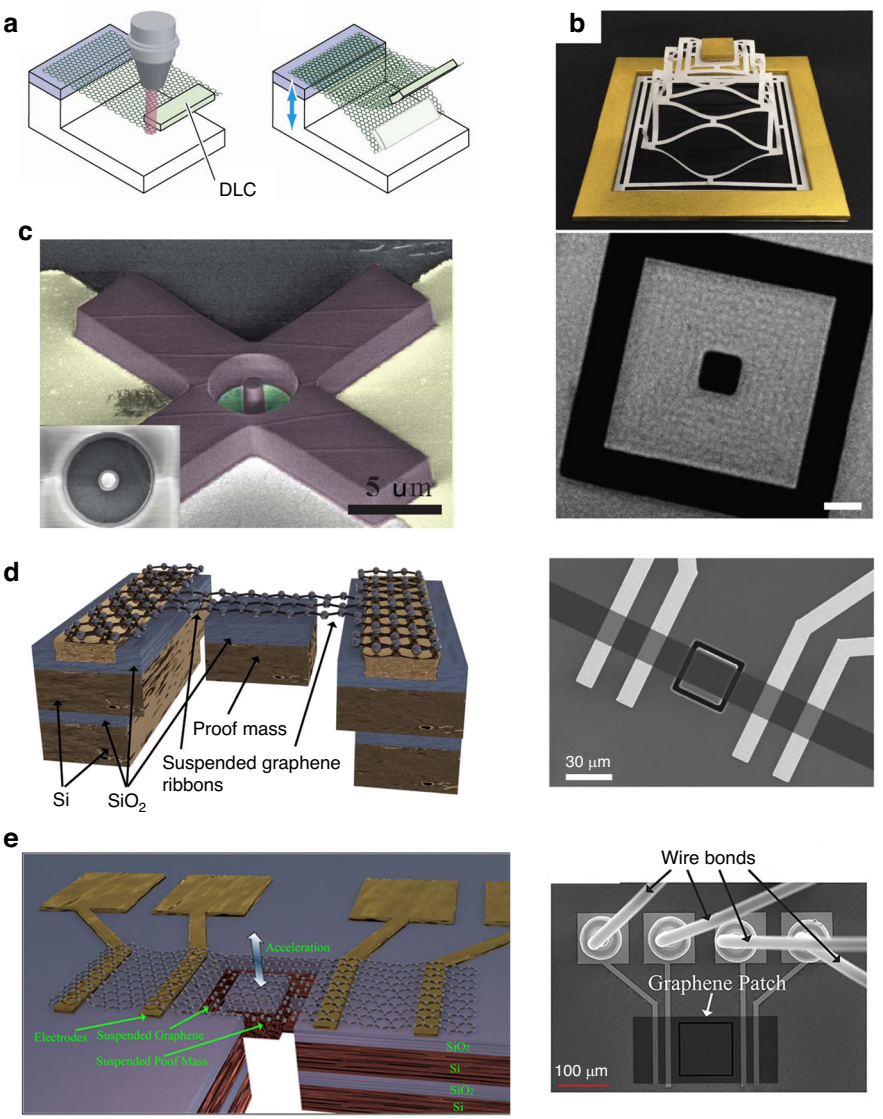

Fig. 14 Suspended graphene with an attached mass. a A schematic of a few-layer graphene cantilever with diamond-like carbon weights[270]. **b** A schematic of a kirigami pyramid made of suspended graphene supporting gold masses and an SEM image of the as-fabricated graphene kirigami pyramid[271]. **c** An SEM image of a graphene membrane supporting an SU-8 mass[272]. **d** Doubly clamped graphene ribbons with an attached silicon-proof mass as the transducer of the NEMS accelerometers[135]. **e** Fully clamped graphene membranes with attached silicon-proof mass as the transducer of NEMS accelerometers[183]. Figures reproduced with permission from refs. [135,183,270–272]

(LEDs), photovoltaic cells, biomedical sensors, and energy-harvesting devices[277–279]). Compared with traditional transparent conductive electrodes, such as indium tin oxide (ITO), although the sheet resistance of graphene films is still not as low as that of ITO, graphene film-based transparent conductive electrodes are strong, flexible, chemically stable, and can withstand more strain.

Flexible strain sensors

In combination with its transparency, conformal attachment ability, and good stretchability, the sensing features of graphene, such as its piezoresistive properties, make graphene compatible with soft substrates suitable for flexible and wearable sensors, such as strain sensors and pressure sensors. Recently, various types of graphene-based strain sensors that integrate graphene with soft substrates, such as flexible plastic or stretchable rubber substrates (i.e., PDMS), have been widely reported (Fig. 15a–c)[58,71,205,280–287]. For example, highly stretchable strain sensors based on graphene–nanocellulose nanopapers were fabricated by embedding three-dimensional macroporous nanopapers composed of crumpled graphene and nanocellulose in a stretchable elastomer (PDMS), which can respond to strains of up to 100% in all

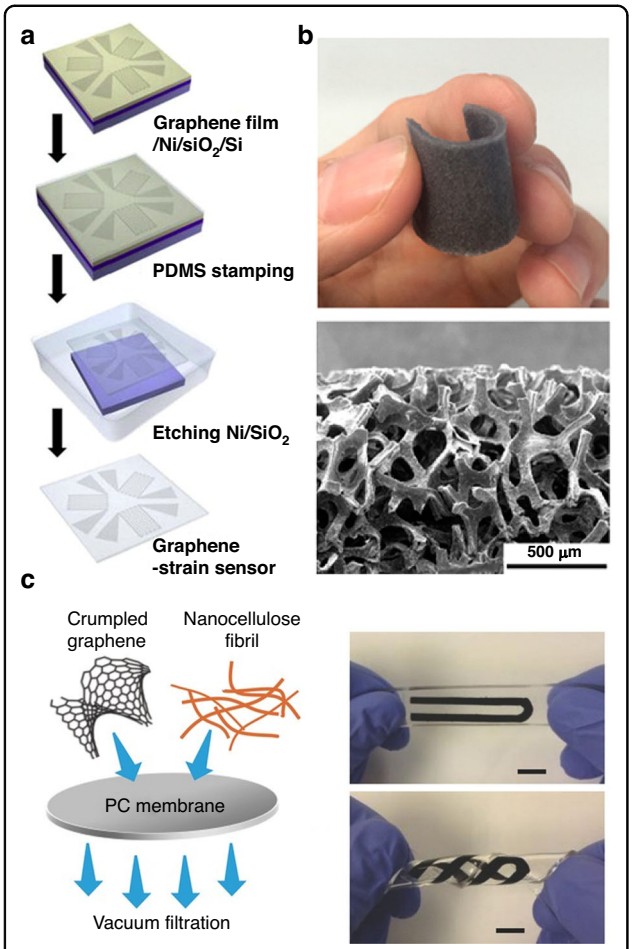

Fig. 15 Flexible strain sensors. a The fabrication process of a graphene strain sensor[284]. **b** A photograph of a bent graphene porous network-PDMS composite and SEM image of nickel foam coated with graphene[286]. **c** A stretchable graphene nanopaper[281]. Figures reproduced with permission from refs. [281,284,286]

directions (Fig. 15c)[281]. The strain sensors described above can detect high strain in human-friendly interactive electronics, such as human joint movement with strains of up to 55%[281]. 3D flexible and conductive composites of graphene foams/PDMS were fabricated by growing graphene foams in a nickel foam substrate that was used as a 3D scaffold template, removing the nickel substrate and infiltrating PDMS into the graphene foam, which can be stretched to 95% before the sample is broken[280]. Furthermore, by using nickel foam as the growth template of graphene, immersing graphene-coated nickel foam into the prepolymer of PDMS, and chemically etching, the porous graphene network combined with PDMS can be used as both a highly sensitive pressure sensor and strain sensor with a wide measurement range for potential applications in monitoring the walking state, degree of finger bending and wrist blood pressure (Fig. 15b)[286]. Nanographene films on PDMS membranes with tunable piezoresistivity for strain sensing with great potential in electronic skin applications can be realized by controlling the nanographene nucleation density and grain size[71].

Flexible pressure sensors

Different types of flexible and wearable graphene-based pressure sensors that use various types of graphene structures together with other materials or soft substrates as sensing layers have also been reported (Fig. 16a, b)[288–291]. For example, pressure sensors based on laser-scribed graphene with a foam-like structure on PET have been reported (Fig. 16a)[289]. The sensing principle of a laser-scribed graphene pressure sensor is based on the resistance change between the bottom and top pieces of laser-scribed graphene films that are composed of loosely stacked graphene layers[289]. The sensor sensitivity is as high as 0.96 kPa^{-1} over a wide pressure sensing range (0–50 kPa) because of the large interspacing between graphene layers and the unique V-shaped microstructure of laser-scribed structures[289]. Furthermore, graphene/paper pressure sensors with the ability to measure the wrist pulse, breathing, and motion states were realized via the reduction of graphene oxide on the tissue paper in the oven at high temperature, with a pressure range of 20 kPa and ultrahigh sensitivity of 17.2 kPa^{-1} (0–2 kPa)[290]. Graphene/PDMS pressure sensors with a random distribution spinosum microstructure were fabricated by using abrasive paper as a template and the thermal reduction of graphene oxide; the sensitivity of these sensors was as high as 25.1 kPa^{-1} over a wide linear range of 0–2.6 kPa (Fig. 16b)[291]. This type of pressure sensor can be used to detect physiological activities, such as human health care monitoring, voice, phonation identification, and motion movement[291].

Flexible audio-emitting and receiving devices

Owing to its ultrathin thickness, excellent mechanical properties, superior thermal conductivity, and low heat capacity per unit area, graphene can be used for flexible sound generators that can produce sound in audible and ultrasound ranges according to the thermoacoustic effect and has potential applications in speakers, buzzers, earphones, ultrasonic detection, and imaging, etc. The basic principle of the thermoacoustic effect can be described as follows: when an alternating current is loaded to a conductor, Joule heating will heat the air near its surface periodically, thereby resulting in the periodic vibration of air and the formation of sound waves. The low heat capacity per unit area of the conductor, which can quickly heat the environment, and the low thermal conductivity of the substrate, which can reduce heat leakage from the substrate, are two key conditions for thermoacoustic sound emission[240]. For example, thermophones made of 20–100-nm-thick

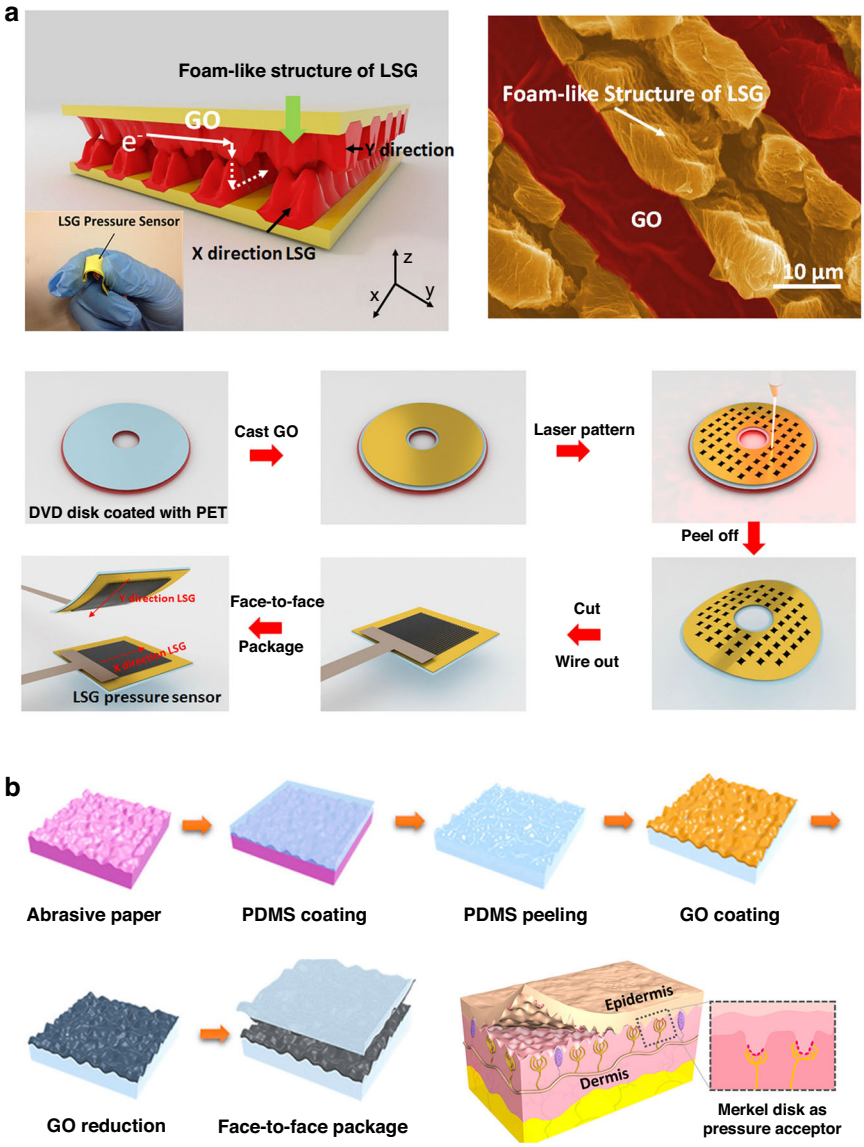

Fig. 16 Flexible pressure sensors. a A laser-scribed graphene-based pressure sensor. This figure part shows a schematic and SEM image of the foam-like structure of laser-scribed graphene and the fabrication process[289]. **b** The fabrication process of a bioinspired graphene pressure sensor with a randomly distributed spinosum microstructure[291]. Figures reproduced with permission from refs. [289,291]

graphene sheets were demonstrated by patterning graphene sheets on paper substrates[240], thus indicating that graphene sheets have a significant flat frequency response in the wide ultrasonic range of 20–50 kHz and that thinner graphene sheets can generate higher sound pressure levels. Furthermore, sound-emitting devices based on monolayer graphene were also realized by transferring monolayer graphene onto the substrate of anodic aluminum oxide templates, which therefore reduced heat leakage from the substrate[241].

Combined with the lower heat capacity per unit area of monolayer graphene, monolayer graphene devices can produce higher sound pressures than can graphene sheets. To study the effect of the substrate on sound performance and improve mechanical robustness, double-layer or trilayer graphene was transferred to patterned substrates with different surface porosities, thus indicating that the highest sound pressure was produced from the samples on the substrate with the highest porosity, thereby reducing the heat loss to the supporting substrate as much as possible[292]. In addition to the low heat capacity per unit area of monolayer graphene, the high transmittance and high stretchability of monolayer graphene also allow it to be easily integrated on various transparent supporting substrates, such as PET and PDMS, for transparent and flexible

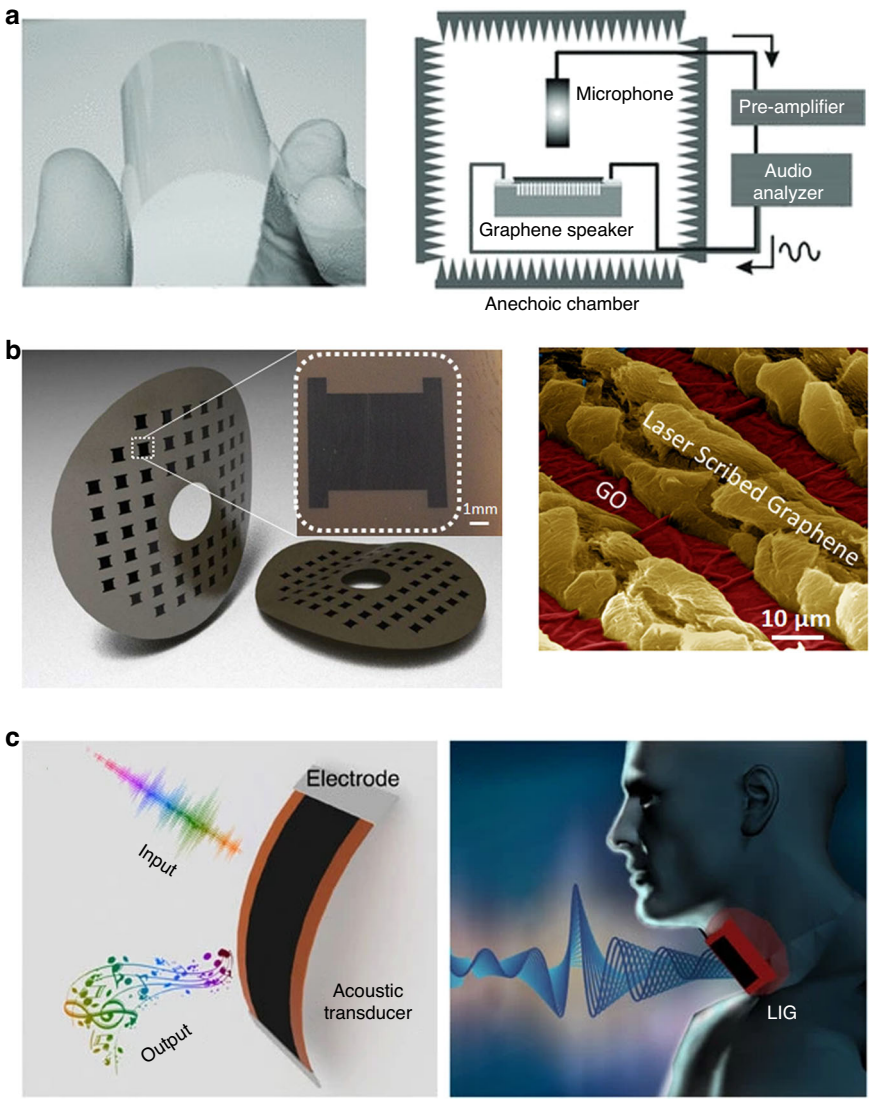

Fig. 17 Flexible audio-emitting and audio-receiving devices based on nonsuspended graphene. a Transparent and flexible graphene-based sound sources, including monolayer graphene on PET and a schematic of the acoustic measurement[292]. **b** Wafer-scale flexible graphene earphones and an SEM image of laser-scribed graphene and graphene oxide[206]. **c** An intelligent artificial throat with sound-sensing ability based on laser-induced graphene[293]. Figures reproduced with permission from refs. [206,292,293]

thermoacoustic sound-emitting devices (Fig. 17a)[292]. Wafer-scale flexible graphene earphones based on reduced-graphene oxide on PET can be realized via laser scribing technology and have a wider frequency response ranging from 100 Hz to 50 kHz, which are suitable for both humans and animals (Fig. 17b)[206]. In addition, graphene samples can be used to sense sound according to sound pressure-induced resistance changes of graphene. For example, a flexible intelligent artificial throat made of porous graphene films on a polyimide substrate via laser scribing technology can both generate and detect sound and thus has the potential to assist the disabled (Fig. 17c)[293].

Flexible actuators

Actuators based on the combination of graphene with conventional membranes have been studied; these actuators have both potential advantages (including large displacement, rapid response at low voltages, flexibility, patternability, and optical transparency) and potential applications (including biomimetic actuators, membranes, and skins). Graphene has a distinctive negative coefficient of thermal expansion (contraction upon heating), which is in contrast with the normal behavior of conventional materials. In addition, graphene has high thermal conductivity. Therefore, a graphene layer can be coupled to different material layers to build microactuators according

to the asymmetric thermomechanical response-induced deflection between two different layers upon heating. For example, hybrid bimorph cantilever microactuators based on serpentine graphene sheets pattern/epoxy (SU-8) were realized via batch microfabrication and can be electromechanically driven by applying electrical power, thus resulting in a large displacement of the cantilever, rapid response and low power consumption (Fig. 18a)[294]. On the basis of the obvious difference in the coefficient of thermal expansion between graphene paper and graphene oxide paper, an electrothermal hybrid cantilever actuator using graphene and graphene oxide composite paper as building blocks can generate a large displacement with low power consumption by bending the cantilever due to thermal stress during the process of applying an electrical voltage[295].

There are other actuating mechanisms for graphene-based actuators. An actuator composed of multiple stacked graphene electrodes and a dielectric elastomer substrate sandwiched between graphene electrodes showed a displacement of 1050 μm at a frequency of 0.5 Hz with a driving voltage of 2 kV[296]. When a voltage was applied, the area of the dielectric elastomer film with sandwiched graphene electrodes contracted in thickness due to the Maxwell stress because of electrostatic charges and extended along the lateral direction[296]. In addition, bilayer paper samples composed of crisscrossed multiwalled CNTs and graphene oxide platelets were used as the building blocks of microactuators[297], in which graphene oxide could mechanically respond to changes in humidity and/or temperature via changes in the amount of interlamellar water between the graphene oxide platelets. Recently, inspired by origami fabrication, using 2D atomic membranes as a folding material, ultrathin microsized graphene–glass bimorph actuators based on strain control mechanisms of temperature or electrolyte concentration were made by bonding CVD graphene sheets to nanometer-thick layers of glass (Fig. 18b)[298].

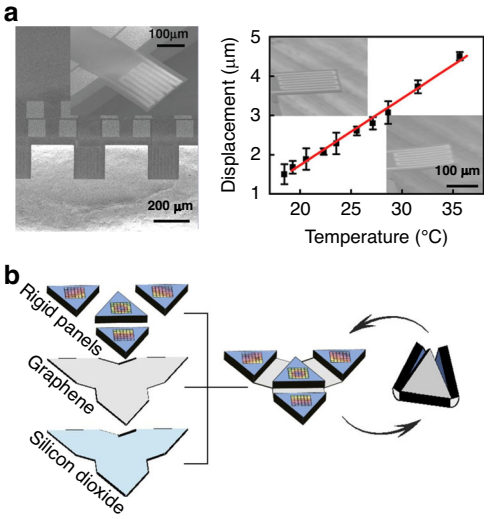

Fig. 18 Flexible actuators based on nonsuspended graphene. a A graphene-based bimorph microactuator with a graphene serpentine pattern and an epoxy hybrid microcantilever[294]. **b** The basic structure of a graphene–glass bimorph is a sheet of graphene bound to a 2 nm thick layer of glass[298]. Figures reproduced with permission from refs. [294,298]

Hall sensors

Graphene is expected to have the potential to outperform currently available Hall sensor technologies; for example, the current-related sensitivities of graphene-based Hall sensors are much higher than those of state-of-the-art Hall sensors made from silicon and comparable to those of state-of-the-art Hall sensors made from III/V semiconductors[106,299,300]. The current-related sensitivities of Hall sensors based on large-area unprotected CVD graphene on SiO_2 substrates and epitaxial graphene on SiC substrates reach 1200 V/AT[103] and 1020 V/AT[301], respectively. In contrast, the current-related sensitivities of common silicon-based Hall sensors are 6.4 V/AT[302] and 123 V/AT[303].

The graphene Hall devices can present very good linearity over a wide range of magnetic fields, particularly in the voltage range[103]. In addition, the carrier density and mobility of graphene are very weakly affected by temperature; thus, graphene Hall sensors can work linearly over very wide temperature ranges, such as from 1.8 to 400 K, with high sensitivity and low thermal drift[103], thus substantially widening the application range of graphene Hall sensors. The graphene Hall elements can be manufactured on a large scale at low cost by developing methods for growing and transferring high-quality graphene, can be easily integrated with integrated circuits for signal amplification and processing, and can be fabricated on different substrates, all of which make graphene Hall elements potential substitutes for conventional Hall elements.

To avoid the possible contamination of graphene devices from the surrounding environment and to obtain reliable, durable, and high-performance materials for practical applications, the encapsulation of graphene should be considered (Fig. 19a–c)[304]. For example, graphene can be encapsulated by the growth of an Al_2O_3 layer via atomic layer deposition, thus resulting in improved results with low doping levels[305]. Furthermore, graphene can be encapsulated by 2D insulating h-BN, which has a superior interface, a low amount of dangling bonds, and charge traps by van der Waals assembly[36], which are beneficial for high-performance Hall sensor elements. In addition to top encapsulation, h-BN is also very suitable for use as a substrate of

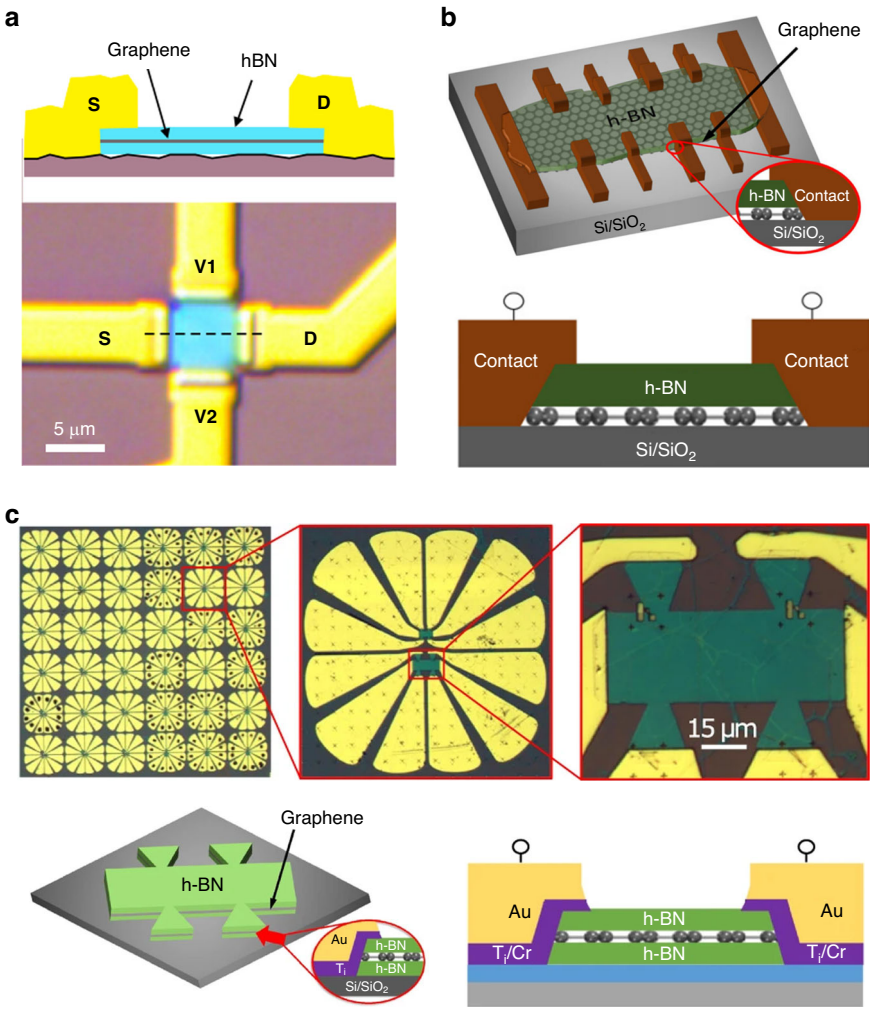

Fig. 19 Hall sensors. a A schematic of a cross-section and an optical image of a Hall sensor based on graphene encapsulated in h-BN[299]. **b** Hall sensors fabricated on large-area CVD graphene protected by h-BN with 1D edge contacts[304]. **c** A batch-fabricated chip and an individual Hall element with an h-BN/graphene/h-BN heterostructure[307]. Figures reproduced with permission from refs. [299,304,307]

graphene in Hall sensor elements for improved performance because of its smoothness. Current-related sensitivities of ~1986 V/AT, 2270 V/AT, and 5700 V/AT were obtained from batch-fabricated CVD graphene on CVD h-BN substrates without top encapsulation[306], CVD graphene patches encapsulated between exfoliated h-BN[107] and stacks of all-exfoliated h-BN/graphene/h-BN[299], respectively. For more practical applications, graphene-based Hall sensors should be manufactured by using all-CVD-grown 2D material heterostructures in a scalable process to fully encapsulate the active region of graphene (Fig. 19c)[307]. In addition to the improved sensitivities, the high linearity[103,106], low noise[106,108,109], wide temperature ranges, thermal stability[103] of the devices, and the transparency and flexibility[107,110], also make graphene attractive for use in magnetic Hall sensors.

Conclusions and outlook

The quality of graphene materials and their commercial availability will mature during the coming years[308–311], thus opening up new exciting applications of graphene in MEMS and NEMS and sensor applications, including flexible and stretchable devices for wearable sensors[43,279]. Graphene is thinner than any currently available CMOS or MEMS/NEMS material and thus could substantially reduce device size while increasing sensitivity. In addition to graphene, many 2D materials (e.g., graphane, fluorographene, h-BN, MoS_2, and other transition metal dichalcogenides (TMDs)) with various exceptional properties, such as from electrically insulating to conductive and from strong to soft, are emerging. For example, some 2D materials have interesting electrical and mechanical properties, such as piezoelectric behavior and a strong piezoresistive effect in MoS_2-based TMDs[312–314]. Although the research on

emerging 2D materials is not mature, and a number of 2D materials are chemically unstable under atmospheric conditions, some of these 2D materials have already been used for sensing applications[315,316]. These emerging 2D materials also have great potential for use in MEMS and NEMS and sensor applications in the future, with the expectation of a substantial reduction in the sizes of the NEMS sensors and improved sensitivity. Furthermore, heterostructures of 2D materials[317,318] and sandwich structures made of two, three, or more economical layers of different 2D materials can provide more opportunities to optimize the properties and structures of materials with atomic precision, possibly yielding more possible applications, including various future MEMS/NEMS and sensor applications.

In this review, we provide an overview of the demonstrated NEMS sensors and proof-of-concept devices based on graphene. These devices are generally smaller than their conventional MEMS counterparts. Furthermore, they showed improved performance and sometimes even completely novel functionalities. However, there are still some challenges for graphene-based NEMS sensors. We believe that one of the greatest challenges that graphene-based NEMS sensors face is the relatively low-yield manufacturing capabilities of suspended graphene structures. Especially for suspended monolayer graphene structures, the yield is generally quite low. We have provided an overview of potential manufacturing approaches. In addition to different manufacturing approaches that might result in a low yield of suspended graphene, the low yield can essentially be attributed to the grain boundaries and related defects in CVD-grown graphene, which easily result in the fracture of suspended graphene. To improve the yield of the suspended graphene, the CVD method for growing graphene should be continuously improved so that sufficiently large grains of graphene with as few grain boundaries as possible can be realized. Other solutions for improving the yield of suspended graphene include the continuous improvement of graphene transfer methods, the use of BHF etching followed by CPD or the use of HF vapor to release graphene for suspension, and the use of two to ten atomic layers of graphene or stacks of graphene with polymers or other membranes.

Another of the greatest challenges that graphene-based NEMS sensors face is their relatively poor stability and reliability. The electrical signal from practical graphene-based NEMS sensors, especially monolayer graphene-based devices, is extremely sensitive to various environmental parameters, such as humidity, gas, temperature, and electromagnetic fields, thus resulting in relatively poor stability and reliability. To address this challenge, graphene should be carefully shielded from environmental influences. For example, graphene can be encapsulated by other membranes, such as h-BN, Si_3N_4, Al_2O_3, or PMMA-based polymers.

In addition, developing a feasible approach for manufacturing multiple types of suspended sensors in a single fabrication flow is highly important and is a typical challenge. Other challenges include high-performance electronic readout circuits, packaging, and reliability measurements for graphene-based NEMS devices.

Acknowledgements
This work was supported by the National Natural Science Foundation of China (62171037 and 62088101), the 173 Technical Field Fund (2023-JCJQ-JJ-0971), the Beijing Natural Science Foundation (4232076), the National Key Research and Development Program of China (2022YFB3204600), the Beijing Institute of Technology Science and Technology Innovation Plan (2022CX11019), the National Science Fund for Excellent Young Scholars (Overseas), the Beijing Institute of Technology Teli Young Fellow Program (2021TLQT012), and the FLAG-ERA project 2DNEMS funded by the Swedish Research Council (VR) (2019-03412).

Author details
[1]Advanced Research Institute of Multidisciplinary Sciences, Beijing Institute of Technology, 100081 Beijing, China. [2]Center for Interdisciplinary Science of Optical Quantum and NEMS Integration, School of Physics, Beijing Institute of Technology, 100081 Beijing, China. [3]School of Integrated Circuits and Electronics, Beijing Institute of Technology, 100081 Beijing, China. [4]Chair of Electronic Devices, Faculty of Electrical Engineering and Information Technology, RWTH Aachen University, Otto-Blumenthal-Str. 25, 52074 Aachen, Germany. [5]AMO GmbH, Otto-Blumenthal-Str. 25, 52074 Aachen, Germany. [6]State Key Laboratory of Dynamic Measurement Technology, North University of China, Taiyuan 030051, China. [7]National Key Laboratory for Electronic Measurement Technology, School of Instrument and Electronics, North University of China, Taiyuan 030051, China

Conflict of interest
The authors declare no competing interests.

Received: 9 June 2024 Revised: 22 July 2024 Accepted: 14 August 2024
Published online: 28 October 2024

References

1. Novoselov, K. S. et al. Electric field effect in atomically thin carbon films. *Science* **306**, 666–669 (2004).
2. Novoselov, K. S. et al. Two-dimensional gas of massless Dirac fermions in graphene. *Nature* **438**, 197 (2005).
3. Allen, M. J., Tung, V. C. & Kaner, R. B. Honeycomb carbon: a review of graphene. *Chem. Rev.* **110**, 132–145 (2010).
4. Bolotin, K. I. et al. Ultrahigh electron mobility in suspended graphene. *Solid State Commun.* **146**, 351–355 (2008).
5. Lee, C., Wei, X., Kysar, J. W. & Hone, J. Measurement of the elastic properties and intrinsic strength of monolayer graphene. *Science* **321**, 385–388 (2008).
6. Zhao, J. et al. Ultrahigh-mobility semiconducting epitaxial graphene on silicon carbide. *Nature* **625**, 60–65 (2024).
7. Novoselov, K. S. et al. A roadmap for graphene. *Nature* **490**, 192–200 (2012).
8. Xiong, G., Meng, C., Reifenberger, R. G., Irazoqui, P. P. & Fisher, T. S. A review of graphene-based electrochemical microsupercapacitors. *Electroanalysis* **26**, 30–51 (2014).
9. Mehta, R., Chugh, S. & Chen, Z. Enhanced electrical and thermal conduction in graphene-encapsulated copper nanowires. *Nano Lett.* **15**, 2024–2030 (2015).
10. Grigorenko, A. N., Polini, M. & Novoselov, K. S. Graphene plasmonics. *Nat. Photonics* **6**, 749–758 (2012).
11. Song, S. H. et al. Enhanced thermal conductivity of epoxy–graphene composites by using non-oxidized graphene flakes with non-covalent functionalization. *Adv. Mater.* **25**, 732–737 (2013).
12. Huang, X., Qi, X., Boey, F. & Zhang, H. Graphene-based composites. *Chem. Soc. Rev.* **41**, 666–686 (2012).

13. Berman, D., Erdemir, A. & Sumant, A. V. Graphene: a new emerging lubricant. *Mater. Today* **17**, 31–42 (2014).
14. Bunch, J. S. et al. Electromechanical resonators from graphene sheets. *Science* **315**, 490–493 (2007).
15. Schedin, F. et al. Detection of individual gas molecules adsorbed on graphene. *Nat. Mater.* **6**, 652–655 (2007).
16. Ma, H. et al. Recent advances in graphene-based humidity sensors with the focus of structural design: a review. *IEEE Sens. J.* https://doi.org/10.1109/JSEN.2024.3398003 (2024).
17. Zhang, Z. et al. Recent advances in graphene-based pressure sensors: a review. *IEEE Sens. J.* https://doi.org/10.1109/JSEN.2024.3419243 (2024).
18. Chen, C. & Hone, J. Graphene nanoelectromechanical systems. *Proc. IEEE* **101**, 1766–1779 (2013).
19. Xu, B. et al. Nanomechanical resonators: toward atomic scale. *ACS Nano* **16**, 15545–15585 (2022).
20. Xiao, Y. et al. A review on graphene-based nano-electromechanical resonators: fabrication, performance, and applications. *Micromachines* **13**, 215 (2022).
21. Zang, X., Zhou, Q., Chang, J., Liu, Y. & Lin, L. Graphene and carbon nanotube (CNT) in MEMS/NEMS applications. *Microelectron. Eng.* **132**, 192–206 (2015).
22. Cho, J. H., Cayll, D., Behera, D. & Cullinan, M. Towards repeatable, scalable graphene integrated micro-nano electromechanical systems (MEMS/NEMS). *Micromachines* **13**, 27 (2021).
23. Lemme, M. C. et al. Nanoelectromechanical sensors based on suspended 2D materials. *Research* **2020**, 2020/8748602 (2020).
24. Bonaccorso, F., Sun, Z., Hasan, T. & Ferrari, A. C. Graphene photonics and optoelectronics. *Nat. Photonics* **4**, 611–622 (2010).
25. Koppens, F. H. L. et al. Photodetectors based on graphene, other two-dimensional materials and hybrid systems. *Nat. Nanotechnol.* **9**, 780–793 (2014).
26. Ferrari, A. C. et al. Science and technology roadmap for graphene, related two-dimensional crystals, and hybrid systems. *Nanoscale* **7**, 4598–4810 (2015).
27. Mayorov, A. S. et al. Micrometer-scale ballistic transport in encapsulated graphene at room temperature. *Nano Lett.* **11**, 2396–2399 (2011).
28. Balandin, A. A. Thermal properties of graphene and nanostructured carbon materials. *Nat. Mater.* **10**, 569–581 (2011).
29. Nair, R. R. et al. Fine structure constant defines visual transparency of graphene. *Science* **320**, 1308–1308 (2008).
30. Bunch, J. S. et al. Impermeable atomic membranes from graphene sheets. *Nano Lett.* **8**, 2458–2462 (2008).
31. Tomori, H. et al. Introducing nonuniform strain to graphene using dielectric nanopillars. *Appl. Phys. Express* **4**, 075102 (2011).
32. Moser, J., Barreiro, A. & Bachtold, A. Current-induced cleaning of graphene. *Appl. Phys. Lett.* **91**, 163513 (2007).
33. Koenig, S. P., Boddeti, N. G., Dunn, M. L. & Bunch, J. S. Ultrastrong adhesion of graphene membranes. *Nat. Nanotechnol.* **6**, 543–546 (2011).
34. Smith, A. D. et al. Electromechanical piezoresistive sensing in suspended graphene membranes. *Nano Lett.* **13**, 3237–3242 (2013).
35. Axet, M. R., Dechy-Cabaret, O., Durand, J., Gouygou, M. & Serp, P. Coordination chemistry on carbon surfaces. *Coord. Chem. Rev.* **308**, 236–345 (2016).
36. Dean, C. R. et al. Boron nitride substrates for high-quality graphene electronics. *Nat. Nanotechnol.* **5**, 722–726 (2010).
37. Nicolosi, V., Chhowalla, M., Kanatzidis, M. G., Strano, M. S. & Coleman, J. N. Liquid exfoliation of layered materials. *Science* **340**, 1226419 (2013).
38. Zheng, J. et al. High yield exfoliation of two-dimensional chalcogenides using sodium naphthalenide. *Nat. Commun.* **5**, 2995 (2014).
39. Hernandez, Y. et al. High-yield production of graphene by liquid-phase exfoliation of graphite. *Nat. Nanotechnol.* **3**, 563–568 (2008).
40. Coleman, J. N. et al. Two-dimensional nanosheets produced by liquid exfoliation of layered materials. *Science* **331**, 568–571 (2011).
41. Kataria, S. et al. Chemical vapor deposited graphene: from synthesis to applications. *Phys. Status Solidi A* **211**, 2439–2449 (2014).
42. Li, X. et al. Large-area synthesis of high-quality and uniform graphene films on copper foils. *Science* **324**, 1312–1314 (2009).
43. Kim, K. S. et al. Large-scale pattern growth of graphene films for stretchable transparent electrodes. *Nature* **457**, 706–710 (2009).
44. Berger, C. et al. Ultrathin epitaxial graphite: 2D electron gas properties and a route toward graphene-based nanoelectronics. *J. Phys. Chem. B* **108**, 19912–19916 (2004).
45. Sutter, P. W., Flege, J.-I. & Sutter, E. A. Epitaxial graphene on ruthenium. *Nat. Mater.* **7**, 406–411 (2008).
46. Yazyev, O. V. & Chen, Y. P. Polycrystalline graphene and other two-dimensional materials. *Nat. Nanotechnol.* **9**, 755–767 (2014).
47. Fan, X. Direct observation of grain boundaries in graphene through vapor hydrofluoric acid (VHF) exposure. *Sci. Adv.* **4**, 5170 (2018).
48. Fan, X., Siris, R., Hartwig, O., Duesberg, G. S. & Niklaus, F. Rapid and large-area visualization of grain boundaries in MoS_2 on SiO_2 using vapor hydrofluoric acid. *ACS Appl. Mater. Interfaces* **12**, 34049–34057 (2020).
49. El-Kady, M. F., Strong, V., Dubin, S. & Kaner, R. B. Laser scribing of high-performance and flexible graphene-based electrochemical capacitors. *Science* **335**, 1326–1330 (2012).
50. Smith, A. D. et al. Resistive graphene humidity sensors with rapid and direct electrical readout. *Nanoscale* **7**, 19099–19109 (2015).
51. Smith, A. D. et al. Graphene-based CO_2 sensing and its cross-sensitivity with humidity. *RSC Adv.* **7**, 22329–22339 (2017).
52. Fan, X. et al. Humidity and CO_2 gas sensing properties of double-layer graphene. *Carbon* **127**, 576–587 (2018).
53. Quellmalz, A. et al. Influence of humidity on contact resistance in graphene devices. *ACS Appl. Mater. Interfaces* **10**, 41738–41746 (2018).
54. Ghosh, A., Late, D. J., Panchakarla, L. S., Govindaraj, A. & Rao, C. N. R. NO_2 and humidity sensing characteristics of few-layer graphenes. *J. Exp. Nanosci.* **4**, 313–322 (2009).
55. Li, M. et al. Temperature characteristics of a pressure sensor based on BN/graphene/BN heterostructure. *Sensors* **19**, 2223 (2019).
56. Irani, F. S. et al. Graphene as a piezoresistive material in strain sensing applications. *Micromachines* **13**, 119 (2022).
57. Zhao, J., Zhang, G.-Y. & Shi, D.-X. Review of graphene-based strain sensors. *Chin. Phys. B* **22**, 057701 (2013).
58. Zhao, J. et al. Ultra-sensitive strain sensors based on piezoresistive nanographene films. *Appl. Phys. Lett.* **101**, 063112 (2012).
59. Wang, Q., Hong, W. & Dong, L. Graphene "microdrums" on a freestanding perforated thin membrane for high sensitivity MEMS pressure sensors. *Nanoscale* **8**, 7663–7671 (2016).
60. Huang, M., Pascal, T. A., Kim, H., Goddard, W. A. & Greer, J. R. Electronic−mechanical coupling in graphene from in situ nanoindentation experiments and multiscale atomistic simulations. *Nano Lett.* **11**, 1241–1246 (2011).
61. Zhu, S.-E., Krishna Ghatkesar, M., Zhang, C. & Janssen, G. C. A. M. Graphene based piezoresistive pressure sensor. *Appl. Phys. Lett.* **102**, 161904 (2013).
62. Lee, Y. et al. Wafer-scale synthesis and transfer of graphene films. *Nano Lett.* **10**, 490–493 (2010).
63. Wang, Y. et al. Super-elastic graphene ripples for flexible strain sensors. *ACS Nano* **5**, 3645–3650 (2011).
64. Benameur, M. M. et al. Electromechanical oscillations in bilayer graphene. *Nat. Commun.* **6**, 8582 (2015).
65. Smith, A. D. et al. Biaxial strain in suspended graphene membranes for piezoresistive sensing. In *2014 IEEE 27th International Conference on Micro Electro Mechanical Systems (MEMS)* 1055–1058 (IEEE, 2014)
66. Zheng, X., Chen, X., Kim, J.-K., Lee, D.-W. & Li, X. Measurement of the gauge factor of few-layer graphene. *J. MicroNanolith. MEMS MOEMS* **12**, 013009 (2013).
67. Chen, X., Zheng, X., Kim, J.-K., Li, X. & Lee, D.-W. Investigation of graphene piezoresistors for use as strain gauge sensors. *J. Vac. Sci. Technol. B* **29**, 06FE01 (2011).
68. Hosseinzadegan, H. et al. Graphene has ultra high piezoresistive gauge factor. In *2012 IEEE 25th International Conference on Micro Electro Mechanical Systems (MEMS)* 611–614 (IEEE, 2012).
69. Pereira, V. M., Castro Neto, A. H. & Peres, N. M. R. Tight-binding approach to uniaxial strain in graphene. *Phys. Rev. B* **80**, 045401 (2009).
70. Smith, A. D. et al. Piezoresistive properties of suspended graphene membranes under uniaxial and biaxial strain in nanoelectromechanical pressure sensors. *ACS Nano* **10**, 9879–9886 (2016).
71. Zhao, J. et al. Tunable piezoresistivity of nanographene films for strain sensing. *ACS Nano* **9**, 1622–1629 (2015).
72. Hempel, M., Nezich, D., Kong, J. & Hofmann, M. A novel class of strain gauges based on layered percolative films of 2D materials. *Nano Lett.* **12**, 5714–5718 (2012).
73. Luo, S., Hoang, P. T. & Liu, T. Direct laser writing for creating porous graphitic structures and their use for flexible and highly sensitive sensor and sensor arrays. *Carbon* **96**, 522–531 (2016).

74. Kim, Y.-J. et al. Preparation of piezoresistive nano smart hybrid material based on graphene. *Curr. Appl. Phys.* **11**, S350–S352 (2011).
75. Li, X. et al. Stretchable and highly sensitive graphene-on-polymer strain sensors. *Sci. Rep.* **2**, 870 (2012).
76. Acquarelli, C., Paliotta, L., Tamburrano, A., De Bellis, G. & Sarto, M. S. Electromechanical properties of multilayer graphene-based polymeric composite obtained through a capillary rise method. *Sensors* **16**, 1780 (2016).
77. Chen, Y.-M. et al. Ultra-large suspended graphene as a highly elastic membrane for capacitive pressure sensors. *Nanoscale* **8**, 3555–3564 (2016).
78. Sharma, B. K. & Ahn, J.-H. Graphene based field effect transistors: efforts made towards flexible electronics. *Solid-State Electron* **89**, 177–188 (2013).
79. Reddy, D., Register, L. F., Carpenter, G. D. & Banerjee, S. K. Graphene field-effect transistors. *J. Phys. Appl. Phys.* **44**, 313001 (2011).
80. Schwierz, F. Graphene transistors. *Nat. Nanotechnol.* **5**, 487–496 (2010).
81. Zhan, B. et al. Graphene field-effect transistor and its application for electronic sensing. *Small* https://doi.org/10.1002/smll.201400463 (2014).
82. Fardindoost, S. et al. Flexible strain sensors based on electrostatically actuated graphene flakes. *J. Micromech. Microeng.* **25**, 075016 (2015).
83. Milaninia, K. M., Baldo, M. A., Reina, A. & Kong, J. All graphene electromechanical switch fabricated by chemical vapor deposition. *Appl. Phys. Lett.* **95**, 183105 (2009).
84. Kim, S. M. et al. Suspended few-layer graphene beam electromechanical switch with abrupt on-off characteristics and minimal leakage current. *Appl. Phys. Lett.* **99**, 023103 (2011).
85. Nagase, M., Hibino, H., Kageshima, H. & Yamaguchi, H. Graphene-based nano-electro-mechanical switch with high on/off ratio. *Appl. Phys. Express* **6**, 055101 (2013).
86. Li, P., You, Z., Haugstad, G. & Cui, T. Graphene fixed-end beam arrays based on mechanical exfoliation. *Appl. Phys. Lett.* **98**, 253105 (2011).
87. Sun, J., Wang, W., Muruganathan, M. & Mizuta, H. Low pull-in voltage graphene electromechanical switch fabricated with a polymer sacrificial spacer. *Appl. Phys. Lett.* **105**, 033103 (2014).
88. Li, P., You, Z. & Cui, T. Raman spectrum method for characterization of pull-in voltages of graphene capacitive shunt switches. *Appl. Phys. Lett.* **101**, 263103 (2012).
89. Li, P., You, Z. & Cui, T. Graphene cantilever beams for nano switches. *Appl. Phys. Lett.* **101**, 093111 (2012).
90. Reserbat-Plantey, A., Marty, L., Arcizet, O., Bendiab, N. & Bouchiat, V. A local optical probe for measuring motion and stress in a nanoelectromechanical system. *Nat. Nanotechnol.* **7**, 151–155 (2012).
91. Liu, X. et al. Large arrays and properties of 3-terminal graphene nanoelectromechanical switches. *Adv. Mater.* **26**, 1571–1576 (2014).
92. Sun, J., Muruganathan, M., Kanetake, N. & Mizuta, H. Locally-actuated graphene-based nano-electro-mechanical switch. *Micromachines* **7**, 124 (2016).
93. Sun, J., Schmidt, M. E., Muruganathan, M., Chong, H. M. H. & Mizuta, H. Large-scale nanoelectromechanical switches based on directly deposited nanocrystalline graphene on insulating substrates. *Nanoscale* **8**, 6659–6665 (2016).
94. Zhou, Q. & Zettl, A. Electrostatic graphene loudspeaker. *Appl. Phys. Lett.* **102**, 223109 (2013).
95. Zhou, Q., Zheng, J., Onishi, S., Crommie, M. F. & Zettl, A. K. Graphene electrostatic microphone and ultrasonic radio. *Proc. Natl Acad. Sci. USA* **112**, 8942–8946 (2015).
96. Dolleman, R. J., Davidovikj, D., Cartamil-Bueno, S. J., van der Zant, H. S. J. & Steeneken, P. G. Graphene squeeze-film pressure sensors. *Nano Lett.* **16**, 568–571 (2016).
97. Robinson, J. T. et al. Wafer-scale reduced graphene oxide films for nanomechanical devices. *Nano Lett.* **8**, 3441–3445 (2008).
98. Shivaraman, S. et al. Free-standing epitaxial graphene. *Nano Lett.* **9**, 3100–3105 (2009).
99. van der Zande, A. M. et al. Large-scale arrays of single-layer graphene resonators. *Nano Lett.* **10**, 4869–4873 (2010).
100. Barton, R. A. et al. High, size-dependent quality factor in an array of graphene mechanical resonators. *Nano Lett.* **11**, 1232–1236 (2011).
101. Ripka, P. *Magnetic Sensors and Magnetometers* (Aretech House, 2001).
102. Popovic, R. S. *Hall Effect Devices* (CRC Press, 2003)
103. Xu, H. et al. Batch-fabricated high-performance graphene Hall elements. *Sci. Rep.* **3**, 1207 (2013).
104. Boero, G., Demierre, M., Besse, P.-A. & Popovic, R. S. Micro-Hall devices: performance, technologies and applications. *Sens. Actuators Phys.* **106**, 314–320 (2003).
105. Heremans, J. Solid state magnetic field sensors and applications. *J. Phys. Appl. Phys.* **26**, 1149–1168 (1993).
106. Huang, L. et al. Ultra-sensitive graphene Hall elements. *Appl. Phys. Lett.* **104**, 183106 (2014).
107. Wang, Z. et al. Encapsulated graphene-based Hall sensors on foil with increased sensitivity: encapsulated graphene-based Hall sensors. *Phys. Status Solidi B* **253**, 2316–2320 (2016).
108. Xu, H. et al. Flicker noise and magnetic resolution of graphene hall sensors at low frequency. *Appl. Phys. Lett.* **103**, 112405 (2013).
109. Ciuk, T. et al. Low-noise epitaxial graphene on SiC Hall effect element for commercial applications. *Appl. Phys. Lett.* **108**, 223504 (2016).
110. Wang, Z., Shaygan, M., Otto, M., Schall, D. & Neumaier, D. Flexible Hall sensors based on graphene. *Nanoscale* **8**, 7683–7687 (2016).
111. Wang, X. et al. Observation of a giant two-dimensional band-piezoelectric effect on biaxial-strained graphene. *NPG Asia Mater.* **7**, e154 (2015).
112. Da Cunha Rodrigues, G. et al. Strong piezoelectricity in single-layer graphene deposited on SiO2 grating substrates. *Nat. Commun.* **6**, 7572 (2015).
113. Bao, W. et al. In situ observation of electrostatic and thermal manipulation of suspended graphene membranes. *Nano Lett.* **12**, 5470–5474 (2012).
114. Smith, A. D. et al. Toward effective passivation of graphene to humidity sensing effects. In *2016 46th European Solid-State Device Research Conference (ESSDERC)* 299–302 (IEEE, 2016).
115. Kwon, B. et al. Ultrasensitive N-channel graphene gas sensors by non-destructive molecular doping. *ACS Nano* **16**, 2176–2187 (2022).
116. Leenaerts, O., Partoens, B. & Peeters, F. Adsorption of H2O, NH3, CO, NO2, and NO on graphene: a first-principles study. *Phys. Rev. B* **77**, 125416 (2008).
117. Leenaerts, O., Partoens, B. & Peeters, F. M. Adsorption of small molecules on graphene. *Microelectron. J.* **40**, 860–862 (2009).
118. Zhang, Y.-H. et al. Improving gas sensing properties of graphene by introducing dopants and defects: a first-principles study. *Nanotechnology* **20**, 185504 (2009).
119. Li, G. et al. High-sensitivity MEMS force and acceleration sensor based on graphene-induced non-radiative transition. *Carbon* **209**, 118001 (2023).
120. Wang, Z. et al. A high-temperature accelerometer with excellent performance based on the improved graphene aerogel. *ACS Appl. Mater. Interfaces* **15**, 19337–19348 (2023).
121. Zhang, Y., Small, J. P., Pontius, W. V. & Kim, P. Fabrication and electric-field-dependent transport measurements of mesoscopic graphite devices. *Appl. Phys. Lett.* **86**, 073104 (2005).
122. Huang, Y. et al. Universal mechanical exfoliation of large-area 2D crystals. *Nat. Commun.* **11**, 2453 (2020).
123. Huang, Y. et al. Reliable exfoliation of large-area high-quality flakes of graphene and other two-dimensional materials. *ACS Nano* **9**, 10612–10620 (2015).
124. Unarunotai, S. et al. Transfer of graphene layers grown on SiC wafers to other substrates and their integration into field effect transistors. *Appl. Phys. Lett.* **95**, 202101 (2009).
125. Unarunotai, S. et al. Layer-by-layer transfer of multiple, large area sheets of graphene grown in multilayer stacks on a single SiC wafer. *ACS Nano* **4**, 5591–5598 (2010).
126. Caldwell, J. D. et al. Technique for the dry transfer of epitaxial graphene onto arbitrary substrates. *ACS Nano* **4**, 1108–1114 (2010).
127. Lee, D. S. et al. Raman spectra of epitaxial graphene on SiC and of epitaxial graphene transferred to SiO_2. *Nano Lett.* **8**, 4320–4325 (2008).
128. Tanabe, S., Furukawa, K. & Hibino, H. Etchant-free and damageless transfer of monolayer and bilayer graphene grown on SiC. *Jpn. J. Appl. Phys.* **53**, 115101 (2014).
129. Gao, L. et al. Face-to-face transfer of wafer-scale graphene films. *Nature* **505**, 190–194 (2014).
130. Jiao, L. et al. Creation of nanostructures with poly(methyl methacrylate)-mediated nanotransfer printing. *J. Am. Chem. Soc.* **130**, 12612–12613 (2008).
131. Liang, X. et al. Toward clean and crackless transfer of graphene. *ACS Nano* **5**, 9144–9153 (2011).
132. Li, X. et al. Transfer of large-area graphene films for high-performance transparent conductive electrodes. *Nano Lett.* **9**, 4359–4363 (2009).
133. Suk, J. W. et al. Transfer of CVD-grown monolayer graphene onto arbitrary substrates. *ACS Nano* **5**, 6916–6924 (2011).
134. Fan, X. et al. Direct observation of grain boundaries in graphene through vapor hydrofluoric acid (VHF) exposure. *Sci. Adv.* **4**, eaar5170 (2018).

135. Fan, X. et al. Graphene ribbons with suspended masses as transducers in ultra-small nanoelectromechanical accelerometers. *Nat. Electron.* **2**, 394–404 (2019).
136. Fan, X. et al. Manufacture and characterization of graphene membranes with suspended silicon proof masses for MEMS and NEMS applications. *Microsyst. Nanoeng.* **6**, 17 (2020).
137. Ruiz-Vargas, C. S. et al. Softened elastic response and unzipping in chemical vapor deposition graphene membranes. *Nano Lett.* **11**, 2259–2263 (2011).
138. Suk, J. W. et al. Enhancement of the electrical properties of graphene grown by chemical vapor deposition via controlling the effects of polymer residue. *Nano Lett.* **13**, 1462–1467 (2013).
139. Lee, J. et al. Crack-release transfer method of wafer-scale grown graphene onto large-area substrates. *ACS Appl. Mater. Interfaces* **6**, 12588–12593 (2014).
140. Han, Y. et al. Clean surface transfer of graphene films via an effective sandwich method for organic light-emitting diode applications. *J. Mater. Chem. C.* **2**, 201–207 (2014).
141. Jeong, H. J. et al. Improved transfer of chemical-vapor-deposited graphene through modification of intermolecular interactions and solubility of poly(-methylmethacrylate) layers. *Carbon* **66**, 612–618 (2014).
142. Lin, Y.-C. et al. Clean transfer of graphene for isolation and suspension. *ACS Nano* **5**, 2362–2368 (2011).
143. Song, J. et al. A general method for transferring graphene onto soft surfaces. *Nat. Nanotechnol.* **8**, 356–362 (2013).
144. Kim, H. H. et al. Clean transfer of wafer-scale graphene via liquid phase removal of polycyclic aromatic hydrocarbons. *ACS Nano* **9**, 4726–4733 (2015).
145. Carvalho, A. F. et al. Millimeter-sized few-layer suspended graphene membranes. *Appl. Mater. Today* **21**, 100879 (2020).
146. Leong, W. S. et al. Paraffin-enabled graphene transfer. *Nat. Commun.* **10**, 867 (2019).
147. Liao, J. et al. Crack-free transfer of graphene wafers via photoresist as transfer medium. *Acta Phys. Chim. Sin.* **0**, 2306038 (2023).
148. Shahzad, K. et al. An improved rosin transfer process for the reduction of residue particles for graphene. *Nanoscale Res. Lett.* **15**, 85 (2020).
149. Nakatani, M. et al. Ready-to-transfer two-dimensional materials using tunable adhesive force tapes. *Nat. Electron.* **7**, 119–130 (2024).
150. Bae, S. et al. Roll-to-roll production of 30-inch graphene films for transparent electrodes. *Nat. Nanotechnol.* **5**, 574–578 (2010).
151. Huang, Y. et al. An efficient route to prepare suspended monolayer for feasible optical and electronic characterizations of two-dimensional materials. *InfoMat* **4**, e12274 (2022).
152. Kim, J.-W. et al. Clean and less defective transfer of monolayer graphene by floatation in hot water. *Appl. Surf. Sci.* **508**, 145057 (2020).
153. Wang, Y. et al. Electrochemical delamination of CVD-grown graphene film: toward the recyclable use of copper catalyst. *ACS Nano* **5**, 9927–9933 (2011).
154. De La Rosa, C. J. L. et al. Frame assisted H_2O electrolysis induced H_2 bubbling transfer of large area graphene grown by chemical vapor deposition on Cu. *Appl. Phys. Lett.* **102**, 022101 (2013).
155. Cherian, C. T. et al. Bubble-free' electrochemical delamination of CVD graphene films. *Small* **11**, 189–194 (2015).
156. Pizzocchero, F. et al. Non-destructive electrochemical graphene transfer from reusable thin-film catalysts. *Carbon* **85**, 397–405 (2015).
157. Ren, Y. et al. An improved method for transferring graphene grown by chemical vapor deposition. *Nano* **07**, 1150001 (2012).
158. Lin, W.-H. et al. A direct and polymer-free method for transferring graphene grown by chemical vapor deposition to any substrate. *ACS Nano* **8**, 1784–1791 (2014).
159. Pasternak, I. et al. Graphene films transfer using marker-frame method. *AIP Adv.* **4**, 097133 (2014).
160. Wang, D.-Y. et al. Clean-lifting transfer of large-area residual-free graphene films. *Adv. Mater.* **25**, 4521–4526 (2013).
161. Kim, Y. et al. Influence of the transfer and chemical treatment of monolayer graphene grown for flexible transparent electrodes. *Carbon* **81**, 458–464 (2015).
162. Fechine, G. J. M. et al. Direct dry transfer of chemical vapor deposition graphene to polymeric substrates. *Carbon* **83**, 224–231 (2015).
163. Kim, H. H., Chung, Y., Lee, E., Lee, S. K. & Cho, K. Water-free transfer method for CVD-grown graphene and Its application to flexible air-stable graphene transistors. *Adv. Mater.* **26**, 3213–3217 (2014).
164. Feng, Y. & Chen, K. Dry transfer of chemical-vapor-deposition-grown graphene onto liquid-sensitive surfaces for tunnel junction applications. *Nanotechnology* **26**, 035302 (2015).
165. Kang, J. et al. Efficient transfer of large-area graphene films onto rigid substrates by hot pressing. *ACS Nano* **6**, 5360–5365 (2012).
166. Zaretski, A. V. et al. Metal-assisted exfoliation (MAE): green, roll-to-roll compatible method for transferring graphene to flexible substrates. *Nanotechnology* **26**, 045301 (2015).
167. Kinoshita, K. et al. Dry release transfer of graphene and few-layer h-BN by utilizing thermoplasticity of polypropylene carbonate. *Npj 2D Mater. Appl.* **3**, 22 (2019).
168. Satterthwaite, P. F. et al. Van der Waals device integration beyond the limits of van der Waals forces using adhesive matrix transfer. *Nat. Electron.* **7**, 17–28 (2023).
169. Afyouni Akbari, S., Ghafarinia, V., Larsen, T., Parmar, M. M. & Villanueva, L. G. Large suspended monolayer and bilayer graphene membranes with diameter up to 750 μm. *Sci. Rep.* **10**, 6426 (2020).
170. Quellmalz, A. et al. Large-area integration of two-dimensional materials and their heterostructures by wafer bonding. *Nat. Commun.* **12**, 917 (2021).
171. Shivayogimath, A. et al. Do-it-yourself transfer of large-area graphene using an office laminator and water. *Chem. Mater.* **31**, 2328–2336 (2019).
172. Wang, Z. et al. Facile transfer of monolayer graphene onto polyethylene via van der Waals interactions to prepare layered composite membranes. *Polymer* **282**, 126146 (2023).
173. Gao, X. et al. Integrated wafer-scale ultra-flat graphene by gradient surface energy modulation. *Nat. Commun.* **13**, 5410 (2022).
174. Zhao, Y. et al. Large-area transfer of two-dimensional materials free of cracks, contamination and wrinkles via controllable conformal contact. *Nat. Commun.* **13**, 4409 (2022).
175. Hu, Z. et al. Rapid and scalable transfer of large-area graphene wafers. *Adv. Mater.* **35**, 2300621 (2023).
176. Seah, C.-M., Vigolo, B., Chai, S.-P. & Mohamed, A. R. Transfer of wafer-scale graphene onto arbitrary substrates: steps towards the reuse and recycling of the catalyst. *2D Mater.* **5**, 042001 (2018).
177. Yuan, G. et al. Stacking transfer of wafer-scale graphene-based van der Waals superlattices. *Nat. Commun.* **14**, 5457 (2023).
178. Castellanos-Gomez, A., Singh, V., Van Der Zant, H. S. J. & Steele, G. A. Mechanics of freely-suspended ultrathin layered materials: mechanics of 2D materials. *Ann. Phys.* **527**, 27–44 (2015).
179. Barton, R. A., Parpia, J. & Craighead, H. G. Fabrication and performance of graphene nanoelectromechanical systems. *J. Vac. Sci. Technol. B Nanotechnol. Microelectron. Mater. Process. Meas. Phenom.* **29**, 050801 (2011).
180. Oshidari, Y., Hatakeyama, T., Kometani, R., Warisawa, S. & Ishihara, S. High quality factor graphene resonator fabrication using resist shrinkage-induced strain. *Appl. Phys. Express* **5**, 117201 (2012).
181. Tombros, N. et al. Large yield production of high mobility freely suspended graphene electronic devices on a polydimethylglutarimide based organic polymer. *J. Appl. Phys.* **109**, 093702 (2011).
182. Aydin, O. I., Hallam, T., Thomassin, J. L., Mouis, M. & Duesberg, G. S. Interface and strain effects on the fabrication of suspended CVD graphene devices. *Solid-State Electron* **108**, 75–83 (2015).
183. Fan, X. et al. Suspended graphene membranes with attached silicon proof masses as piezoresistive nanoelectromechanical systems accelerometers. *Nano Lett.* **19**, 6788–6799 (2019).
184. In, J. B., Lee, D., Fornasiero, F., Noy, A. & Grigoropoulos, C. P. Laser-assisted simultaneous transfer and patterning of vertically aligned carbon nanotube arrays on polymer substrates for flexible devices. *ACS Nano* **6**, 7858–7866 (2012).
185. Tian, H. et al. Laser directed lithography of asymmetric graphene ribbons on a polydimethylsiloxane trench structure. *Phys. Chem. Chem. Phys.* **15**, 6825 (2013).
186. Yung, K. C. et al. Laser direct patterning of a reduced-graphene oxide transparent circuit on a graphene oxide thin film. *J. Appl. Phys.* **113**, 244903 (2013).
187. Yoo, J.-H., Park, J. B., Ahn, S. & Grigoropoulos, C. P. Laser-induced direct graphene patterning and simultaneous transferring method for graphene sensor platform. *Small* **9**, 4269–4275 (2013).
188. Ye, X. et al. Direct laser fabrication of large-area and patterned graphene at room temperature. *Carbon* **68**, 784–790 (2014).
189. Xiong, W. et al. Direct writing of graphene patterns on insulating substrates under ambient conditions. *Sci. Rep.* **4**, 4892 (2014).

190. Sahin, R., Simsek, E. & Akturk, S. Nanoscale patterning of graphene through femtosecond laser ablation. *Appl. Phys. Lett.* **104**, 053118 (2014).
191. Mashiyama, D., Tobe, T. & Ogino, T. Nanopatterning of suspended graphene films by local catalytic etching using atomic force microscopy equipped with an Ag-coated probe. *J. Phys. Chem. C.* **119**, 11914–11921 (2015).
192. Bell, D. C., Lemme, M. C., Stern, L. A., Williams, J. R. & Marcus, C. M. Precision cutting and patterning of graphene with helium ions. *Nanotechnology* **20**, 455301 (2009).
193. Liu, W., Wei, J., Sun, X. & Yu, H. A study on graphene—metal contact. *Crystals* **3**, 257–274 (2013).
194. Léonard, F. & Talin, A. A. Electrical contacts to one- and two-dimensional nanomaterials. *Nat. Nanotechnol.* **6**, 773–783 (2011).
195. Allain, A., Kang, J., Banerjee, K. & Kis, A. Electrical contacts to two-dimensional semiconductors. *Nat. Mater.* **14**, 1195–1205 (2015).
196. Passi, V. et al. Contact resistance Study of "edge-contacted" metal-graphene interfaces. In *2016 46th European Solid-State Device Research Conference (ESSDERC)* 236–239 (IEEE, 2016).
197. Cusati, T. et al. Understanding the nature of metal-graphene contacts: a theoretical and experimental study. In *2015 IEEE International Electron Devices Meeting (IEDM)* 12.7.1–12.7.4 (IEEE, 2015).
198. Chu, T. & Chen, Z. Understanding the electrical impact of edge contacts in few-layer graphene. *ACS Nano* **8**, 3584–3589 (2014).
199. Smith, J. T., Franklin, A. D., Farmer, D. B. & Dimitrakopoulos, C. D. Reducing contact resistance in graphene devices through contact area patterning. *ACS Nano* **7**, 3661–3667 (2013).
200. Park, H.-Y. et al. Extremely low contact resistance on graphene through n-type doping and edge contact design. *Adv. Mater.* **28**, 864–870 (2016).
201. Chen, C. et al. Performance of monolayer graphene nanomechanical resonators with electrical readout. *Nat. Nanotechnol.* **4**, 861–867 (2009).
202. Keşkekler, A., Bos, V., Aragón, A. M., Steeneken, P. G. & Alijani, F. Multimode nonlinear dynamics of graphene resonators. *Phys. Rev. Appl.* **20**, 064020 (2023).
203. Yao, B. et al. Gate-tunable frequency combs in graphene–nitride microresonators. *Nature* **558**, 410–414 (2018).
204. Zhang, Z. et al. High-sensitivity force sensors based on novel materials. *Adv. Devices Instrum.* **4**, 0019 (2023).
205. Tian, H. et al. Scalable fabrication of high-performance and flexible graphene strain sensors. *Nanoscale* **6**, 699–705 (2014).
206. Tian, H. et al. Graphene earphones: entertainment for both humans and animals. *ACS Nano* **8**, 5883–5890 (2014).
207. Efetov, D. K. et al. Fast thermal relaxation in cavity-coupled graphene bolometers with a Johnson noise read-out. *Nat. Nanotechnol.* **13**, 797–801 (2018).
208. Blaikie, A., Miller, D. & Alemán, B. J. A fast and sensitive room-temperature graphene nanomechanical bolometer. *Nat. Commun.* **10**, 4726 (2019).
209. Sassi, U. et al. Graphene-based mid-infrared room-temperature pyroelectric bolometers with ultrahigh temperature coefficient of resistance. *Nat. Commun.* **8**, 14311 (2017).
210. Wagner, S. et al. Graphene transfer methods for the fabrication of membrane-based NEMS devices. *Microelectron. Eng.* **159**, 108–113 (2016).
211. Smith, A. D. et al. Pressure sensors based on suspended graphene membranes. *Solid-State Electron* **88**, 89–94 (2013).
212. Kumar, M. & Bhaskaran, H. Ultrasensitive room-temperature piezoresistive transduction in graphene-based nanoelectromechanical systems. *Nano Lett.* **15**, 2562–2567 (2015).
213. Berger, C., Phillips, R., Centeno, A., Zurutuza, A. & Vijayaraghavan, A. Capacitive pressure sensing with suspended graphene–polymer heterostructure membranes. *Nanoscale* **9**, 17439–17449 (2017).
214. Berger, C. et al. Touch-mode capacitive pressure sensor with graphene-polymer heterostructure membrane. *2D Mater.* **5**, 015025 (2017).
215. Davidovikj, D., Scheepers, P. H., Zant, H. S. J. & Steeneken, P. G. Static capacitive pressure sensing using a single graphene drum. *ACS Appl Mater. Interfaces* **9**, 43205–43210 (2017).
216. Šiškins, M. et al. Sensitive capacitive pressure sensors based on graphene membrane arrays. *Microsyst. Nanoeng.* **6**, 102 (2020).
217. Xu, J., Wood, G. S., Mastropaolo, E., Newton, M. J. & Cheung, R. Realization of a graphene/PMMA acoustic capacitive sensor released by silicon dioxide sacrificial layer. *ACS Appl. Mater. Interfaces* **13**, 38792–38798 (2021).
218. Vollebregt, S., Dolleman, R. J., Zant, H. S. J., Steeneken, P. G. & Sarro, P. M. Suspended graphene beams with tunable gap for squeeze-film pressure sensing. In *2017 19th International Conference on Solid-State Sensors, Actuators and Microsystems (TRANSDUCERS)* 770–773 (IEEE, 2017).
219. Patel, R. N., Mathew, J. P., Borah, A. & Deshmukh, M. M. Low tension graphene drums for electromechanical pressure sensing. *2D Mater.* **3**, 011003 (2016).
220. Lee, M. et al. Sealing graphene nanodrums. *Nano Lett.* **19**, 5313–5318 (2019).
221. Naik, A. K., Hanay, M. S., Hiebert, W. K., Feng, X. L. & Roukes, M. L. Towards single-molecule nanomechanical mass spectrometry. *Nat. Nanotechnol.* **4**, 445–450 (2009).
222. Chaste, J. et al. A nanomechanical mass sensor with yoctogram resolution. *Nat. Nanotechnol.* **7**, 301–304 (2012).
223. Jensen, K., Kim, K. & Zettl, A. An atomic-resolution nanomechanical mass sensor. *Nat. Nanotechnol.* **3**, 533–537 (2008).
224. Shin, D. H. et al. Graphene nano-electromechanical mass sensor with high resolution at room temperature. *iScience* **26**, 105958 (2023).
225. Hanay, M. S. et al. Inertial imaging with nanomechanical systems. *Nat. Nanotechnol.* **10**, 339–344 (2015).
226. Davidovikj, D. et al. Visualizing the motion of graphene nanodrums. *Nano Lett.* **16**, 2768–2773 (2016).
227. Shi, Z. et al. Studies of graphene-based nanoelectromechanical switches. *Nano Res.* **5**, 82–87 (2012).
228. Chen, M. E. et al. Graphene-based electromechanical thermal switches. *2D Mater.* **8**, 035055 (2021).
229. Todorović, D. Multilayer graphene condenser microphone. *2D Mater.* **2**, 045013 (2015).
230. Woo, S. Realization of a high sensitivity microphone for a hearing aid using a graphene–PMMA laminated diaphragm. *ACS Appl Mater. Interfaces* **9**, 1237–1246 (2017).
231. Xu, S. C. Flexible and transparent graphene-based loudspeakers. *Appl Phys. Lett.* **102**, 151902 (2013).
232. Pezone, R. et al. Highly-sensitive wafer-scale transfer-free graphene MEMS condenser microphones. *Microsyst. Nanoeng.* **10**, 27 (2024).
233. Pezone, R., Baglioni, G., Sarro, P. M., Steeneken, P. G. & Vollebregt, S. Sensitive transfer-free wafer-scale graphene microphones. *ACS Appl. Mater. Interfaces* **14**, 21705–21712 (2022).
234. Laitinen, A. et al. A graphene resonator as an ultrasound detector for generalized Love waves in a polymer film with two level states. *J. Phys. Appl. Phys.* **52**, 24LT02 (2019).
235. Wittmann, S., Glacer, C., Wagner, S., Pindl, S. & Lemme, M. C. Graphene membranes for Hall sensors and microphones integrated with CMOS-compatible processes. *ACS Appl. Nano Mater.* **2**, 5079–5085 (2019).
236. Verbiest, G. J. et al. Detecting ultrasound vibrations with graphene resonators. *Nano Lett.* **18**, 5132–5137 (2018).
237. Pezone, R. et al. Effect of air-loading on the performance limits of graphene microphones. *Appl. Phys. Lett.* **124**, 123503 (2024).
238. Baglioni, G. et al. Ultra-sensitive graphene membranes for microphone applications. *Nanoscale* **15**, 6343–6352 (2023).
239. Woo, S. et al. Realization of a high sensitivity microphone for a hearing aid using a graphene–PMMA laminated diaphragm. *ACS Appl. Mater. Interfaces* **9**, 1237–1246 (2017).
240. Tian, H. et al. Graphene-on-paper sound source devices. *ACS Nano* **5**, 4878–4885 (2011).
241. Tian, H. et al. Single-layer graphene sound-emitting devices: experiments and modeling. *Nanoscale* **4**, 2272 (2012).
242. Romijn, J. et al. Multi-layer graphene pirani pressure sensors. *Nanotechnology* **32**, 335501 (2021).
243. Dolleman, R. J., Cartamil-Bueno, S. J., Zant, H. S. J. V. D. & Steeneken, P. G. Graphene gas osmometers. *2D Mater.* **4**, 011002 (2016).
244. Davidovikj, D., Bouwmeester, D., Van Der Zant, H. S. J. & Steeneken, P. G. Graphene gas pumps. *2D Mater.* **5**, 031009 (2018).
245. Sun, J., Muruganathan, M. & Mizuta, H. Room temperature detection of individual molecular physisorption using suspended bilayer graphene. *Sci. Adv.* **2**, e1501518 (2016).
246. Rosłoń, I. E., Japaridze, A., Steeneken, P. G., Dekker, C. & Alijani, F. Probing nanomotion of single bacteria with graphene drums. *Nat. Nanotechnol.* **17**, 637–642 (2022).
247. Han, S. et al. Nanoelectromechanical temperature sensor based on piezoresistive properties of suspended graphene film. *Nanomaterials* **13**, 1103 (2023).

248. Steeneken, P. G., Dolleman, R. J., Davidovikj, D., Alijani, F. & Van Der Zant, H. S. J. Dynamics of 2D material membranes. *2D Mater.* **8**, 042001 (2021).
249. Rosłoń, I. E. et al. High-frequency gas effusion through nanopores in suspended graphene. *Nat. Commun.* **11**, 6025 (2020).
250. Al-mashaal, A. K. et al. Dynamic behavior of ultra large graphene-based membranes using electrothermal transduction. *Appl. Phys. Lett.* **111**, 243503 (2017).
251. Zhang, Q.-H. et al. Graphene-based nanoelectromechanical periodic array with tunable frequency. *Nano Lett.* **21**, 8571–8578 (2021).
252. Ferrari, P. F., Kim, S. & Van Der Zande, A. M. Dissipation from interlayer friction in graphene nanoelectromechanical resonators. *Nano Lett.* **21**, 8058–8065 (2021).
253. More, S. K. & Naik, A. K. Strain engineering of graphene nano-resonator. *J. Micromech. Microeng.* **31**, 045015 (2021).
254. Han, E. et al. Ultrasoft slip-mediated bending in few-layer graphene. *Nat. Mater.* **19**, 305–309 (2020).
255. Papageorgiou, D. G., Kinloch, I. A. & Young, R. J. Mechanical properties of graphene and graphene-based nanocomposites. *Prog. Mater. Sci.* **90**, 75–127 (2017).
256. Davidovikj, D., Poot, M., Cartamil-Bueno, S. J., Van Der Zant, H. S. J. & Steeneken, P. G. On-chip heaters for tension tuning of graphene nanodrums. *Nano Lett.* **18**, 2852–2858 (2018).
257. Goldsche, M. et al. Tailoring mechanically tunable strain fields in graphene. *Nano Lett.* **18**, 1707–1713 (2018).
258. Goldsche, M. et al. Fabrication of comb-drive actuators for straining nanostructured suspended graphene. *Nanotechnology* **29**, 375301 (2018).
259. Lee, G.-H. et al. High-strength chemical-vapor–deposited graphene and grain boundaries. *Science* **340**, 1073–1076 (2013).
260. Davidovikj, D. et al. Nonlinear dynamic characterization of two-dimensional materials. *Nat. Commun.* **8**, 1253 (2017).
261. Gómez-Navarro, C., Burghard, M. & Kern, K. Elastic properties of chemically derived single graphene sheets. *Nano Lett.* **8**, 2045–2049 (2008).
262. Fan, X. & Niklaus, F. Deformation behavior and mechanical properties of suspended double-layer graphene ribbons induced by large atomic force microscopy indentation forces. *Adv. Eng. Mater.* **24**, 2100826 (2022).
263. Sun, P. Z. et al. Limits on gas impermeability of graphene. *Nature* **579**, 229–232 (2020).
264. Guo, L. et al. Covalently functionalized nanopores for highly selective separation of monovalent ions. *Adv. Mater.* **36**, 2307242 (2024).
265. Liu, Y., Zhang, S., Song, R., Zeng, H. & Wang, L. Preanchoring enabled directional modification of atomically thin membrane for high-performance osmotic energy generation. *Nano Lett.* **24**, 26–34 (2024).
266. Wang, L. et al. Fundamental transport mechanisms, fabrication and potential applications of nanoporous atomically thin membranes. *Nat. Nanotechnol.* **12**, 509–522 (2017).
267. Macha, M., Marion, S., Nandigana, V. V. R. & Radenovic, A. 2D materials as an emerging platform for nanopore-based power generation. *Nat. Rev. Mater.* **4**, 588–605 (2019).
268. Rollings, R. C., Kuan, A. T. & Golovchenko, J. A. Ion selectivity of graphene nanopores. *Nat. Commun.* **7**, 11408 (2016).
269. Wang, L. et al. Molecular valves for controlling gas phase transport made from discrete ångström-sized pores in graphene. *Nat. Nanotechnol.* **10**, 785–790 (2015).
270. Matsui, K. et al. Mechanical properties of few layer graphene cantilever. In *2014 IEEE 27th International Conference on Micro Electro Mechanical Systems (MEMS)* 1087–1090 (IEEE, 2014).
271. Blees, M. K. et al. Graphene kirigami. *Nature* **524**, 204–207 (2015).
272. Hurst, A. M., Lee, S., Cha, W. & Hone, J. A graphene accelerometer. In *2015 28th IEEE International Conference on Micro Electro Mechanical Systems (MEMS)* 865–868 (IEEE, 2015).
273. Moreno-Garcia, D. et al. A resonant graphene NEMS vibrometer. *Small* **18**, 2201816 (2022).
274. Moreno, D., Fan, X., Niklaus, F. & Guillermo Villanueva, L. Proof of concept of a graphene-based resonant accelerometer. In *2021 IEEE 34th International Conference on Micro Electro Mechanical Systems (MEMS)* 838–840 (IEEE, 2021).
275. Fan, X. et al. Resonant transducers consisting of graphene ribbons with attached proof masses for NEMS sensors. *ACS Appl. Nano Mater.* **7**, 102–109 (2024).
276. He, C., Ding, J. & Fan, X. Modeling and simulation of graphene-based transducers in NEMS accelerometers. *Micromachines* **15**, 409 (2024).
277. Das, T., Sharma, B. K., Katiyar, A. K. & Ahn, J.-H. Graphene-based flexible and wearable electronics. *J. Semicond.* **39**, 011007 (2018).
278. Han, T.-H., Kim, H., Kwon, S.-J. & Lee, T.-W. Graphene-based flexible electronic devices. *Mater. Sci. Eng. R. Rep.* **118**, 1–43 (2017).
279. Jang, H. et al. Graphene-based flexible and stretchable electronics. *Adv. Mater.* **28**, 4184–4202 (2016).
280. Chen, Z. et al. Three-dimensional flexible and conductive interconnected graphene networks grown by chemical vapour deposition. *Nat. Mater.* **10**, 424–428 (2011).
281. Yan, C. et al. Highly stretchable piezoresistive graphene-nanocellulose nanopaper for strain sensors. *Adv. Mater.* **26**, 2022–2027 (2014).
282. Wang, X. et al. Highly sensitive and stretchable piezoresistive strain sensor based on conductive poly(styrene-butadiene-styrene)/few layer graphene composite fiber. *Compos. Part Appl. Sci. Manuf.* **105**, 291–299 (2018).
283. Eswaraiah, V., Balasubramaniam, K. & Ramaprabhu, S. One-pot synthesis of conducting graphene–polymer composites and their strain sensing application. *Nanoscale* **4**, 1258 (2012).
284. Bae, S.-H. et al. Graphene-based transparent strain sensor. *Carbon* **51**, 236–242 (2013).
285. Luo, S. & Liu, T. SWCNT/graphite nanoplatelet hybrid thin films for self-temperature-compensated, highly sensitive, and extensible piezoresistive sensors. *Adv. Mater.* **25**, 5650–5657 (2013).
286. Pang, Y. et al. Flexible, highly sensitive, and wearable pressure and strain sensors with graphene porous network structure. *ACS Appl. Mater. Interfaces* **8**, 26458–26462 (2016).
287. Tao, L.-Q. et al. Self-adapted and tunable graphene strain sensors for detecting both subtle and large human motions. *Nanoscale* **9**, 8266–8273 (2017).
288. Janczak, D., Słoma, M., Wróblewski, G., Młożniak, A. & Jakubowska, M. Screen-printed resistive pressure sensors containing graphene nanoplatelets and carbon nanotubes. *Sensors* **14**, 17304–17312 (2014).
289. Tian, H. et al. A graphene-based resistive pressure sensor with record-high sensitivity in a wide pressure range. *Sci. Rep.* **5**, 8603 (2015).
290. Tao, L.-Q. et al. Graphene-paper pressure sensor for detecting human motions. *ACS Nano* **11**, 8790–8795 (2017).
291. Pang, Y. et al. Epidermis microstructure inspired graphene pressure sensor with random distributed spinosum for high sensitivity and large linearity. *ACS Nano* **12**, 2346–2354 (2018).
292. Suk, J. W., Kirk, K., Hao, Y., Hall, N. A. & Ruoff, R. S. Thermoacoustic sound generation from monolayer graphene for transparent and flexible sound sources. *Adv. Mater.* **24**, 6342–6347 (2012).
293. Tao, L.-Q. et al. An intelligent artificial throat with sound-sensing ability based on laser induced graphene. *Nat. Commun.* **8**, 14579 (2017).
294. Zhu, S.-E. et al. Graphene-based bimorph microactuators. *Nano Lett.* **11**, 977–981 (2011).
295. Zhou, Y., Bi, H., Xie, X., & Sun, L. Fabrication of graphene based electrothermal cantilever actuator. In *The 8th Annual IEEE International Conference on Nano/Micro Engineered and Molecular Systems* 911–914 (IEEE, 2013).
296. Kim, U. et al. A transparent and stretchable graphene-based actuator for tactile display. *Nanotechnology* **24**, 145501 (2013).
297. Park, S., An, J., Suk, J. W. & Ruoff, R. S. Graphene-based actuators. *Small* **6**, 210–212 (2010).
298. Miskin, M. Z. et al. Graphene-based bimorphs for micron-sized, autonomous origami machines. *Proc. Natl Acad. Sci. USA* **115**, 466–470 (2018).
299. Dauber, J. Ultra-sensitive Hall sensors based on graphene encapsulated in hexagonal boron nitride. *Appl Phys. Lett.* **106**, 193501 (2015).
300. Schaefer, B. T. et al. Magnetic field detection limits for ultraclean graphene Hall sensors. *Nat. Commun.* **11**, 4163 (2020).
301. Panchal, V. et al. Small epitaxial graphene devices for magnetosensing applications. *J. Appl. Phys.* **111**, 07E509 (2012).
302. Pascal, J., Hébrard, L., Kammerer, J.-B., Frick, V. & Blondé, J.-P. First vertical Hall device in standard 0.35 µm CMOS technology. *Sens. Actuators Phys.* **147**, 41–46 (2008).
303. Kammerer, J.-B., Hebrard, L., Frick, V., Poure, P. & Braun, F. Horizontal Hall effect sensor with high maximum absolute sensitivity. In *Proceedings of IEEE Sensors* 785–790 (IEEE, 2002).
304. Karpiak, B., Dankert, A. & Dash, S. P. Gate-tunable Hall sensors on large area CVD graphene protected by h-BN with 1D edge contacts. *J. Appl. Phys.* **122**, 054506 (2017).

305. Alexander-Webber, J. A. et al. Encapsulation of graphene transistors and vertical device integration by interface engineering with atomic layer deposited oxide. *2D Mater.* **4**, 011008 (2016).
306. Joo, M.-K. et al. Large-scale graphene on hexagonal-BN Hall elements: prediction of sensor performance without magnetic field. *ACS Nano* **10**, 8803–8811 (2016).
307. Dankert, A., Karpiak, B. & Dash, S. P. Hall sensors batch-fabricated on all-CVD h-BN/graphene/h-BN heterostructures. *Sci. Rep.* **7**, 15231 (2017).
308. Neumaier, D., Pindl, S. & Lemme, M. C. Integrating graphene into semiconductor fabrication lines. *Nat. Mater.* **18**, 525–529 (2019).
309. 15 years of graphene electronics. *Nat. Electron.* **2**, 369–369 (2019).
310. Akinwande, D. et al. Graphene and two-dimensional materials for silicon technology. *Nature* **573**, 507–518 (2019).
311. Lemme, M. C., Akinwande, D., Huyghebaert, C. & Stampfer, C. 2D materials for future heterogeneous electronics. *Nat. Commun.* **13**, 1392 (2022).
312. Bertolazzi, S., Brivio, J. & Kis, A. Stretching and breaking of ultrathin MoS_2. *ACS Nano* **5**, 9703–9709 (2011).
313. Zhu, H. et al. Observation of piezoelectricity in free-standing monolayer MoS2. *Nat. Nanotechnol.* **10**, 151–155 (2015).
314. Manzeli, S., Allain, A., Ghadimi, A. & Kis, A. Piezoresistivity and strain-induced band gap tuning in atomically thin MoS_2. *Nano Lett.* **15**, 5330–5335 (2015).
315. Late, D. J. et al. Sensing behavior of atomically thin-layered MoS_2 transistors. *ACS Nano* **7**, 4879–4891 (2013).
316. Perkins, F. K. et al. Chemical vapor sensing with monolayer MoS_2. *Nano Lett.* **13**, 668–673 (2013).
317. Lotsch, B. V. Vertical 2D heterostructures. *Annu. Rev. Mater. Res.* **45**, 85–109 (2015).
318. Lim, S. et al. Transparent and stretchable interactive human machine interface based on patterned graphene heterostructures. *Adv. Funct. Mater.* **25**, 375–383 (2015).
319. Pérez Garza, H. H., Kievit, E. W., Schneider, G. F. & Staufer, U. Controlled, reversible, and nondestructive generation of uniaxial extreme strains (>10%) in graphene. *Nano Lett.* **14**, 4107–4113 (2014).
320. Androulidakis, C., Zhang, K., Robertson, M. & Tawfick, S. Tailoring the mechanical properties of 2D materials and heterostructures. *2D Mater.* **5**, 032005 (2018).
321. Banszerus, L. et al. Ultrahigh-mobility graphene devices from chemical vapor deposition on reusable copper. *Sci. Adv.* **1**, e1500222 (2015).
322. Dorgan, V. E., Behnam, A., Conley, H. J., Bolotin, K. I. & Pop, E. High-field electrical and thermal transport in suspended graphene. *Nano Lett.* **13**, 4581–4586 (2013).
323. Zomer, P. J., Dash, S. P., Tombros, N. & van Wees, B. J. A transfer technique for high mobility graphene devices on commercially available hexagonal boron nitride. *Appl. Phys. Lett.* **99**, 232104 (2011).
324. Du, X., Skachko, I., Barker, A. & Andrei, E. Y. Approaching ballistic transport in suspended graphene. *Nat. Nanotechnol.* **3**, 491–495 (2008).
325. Song, Y., Fang, W., Hsu, A. L. & Kong, J. Iron (III) chloride doping of CVD graphene. *Nanotechnology* **25**, 395701 (2014).
326. De, S. & Coleman, J. N. Are there fundamental limitations on the sheet resistance and transmittance of thin graphene films? *ACS Nano* **4**, 2713–2720 (2010).
327. Cai, W. et al. Thermal transport in suspended and supported monolayer graphene grown by chemical vapor deposition. *Nano Lett.* **10**, 1645–1651 (2010).
328. Ghosh, S. et al. Extremely high thermal conductivity of graphene: prospects for thermal management applications in nanoelectronic circuits. *Appl. Phys. Lett.* **92**, 151911 (2008).
329. Balandin, A. A. et al. Superior thermal conductivity of single-layer graphene. *Nano Lett.* **8**, 902–907 (2008).
330. Yoon, D., Son, Y.-W. & Cheong, H. Negative thermal expansion coefficient of graphene measured by Raman spectroscopy. *Nano Lett.* **11**, 3227–3231 (2011).
331. Singh, V. et al. Probing thermal expansion of graphene and modal dispersion at low-temperature using graphene nanoelectromechanical systems resonators. *Nanotechnology* **21**, 165204 (2010).
332. Wirtz, C., Berner, N. C. & Duesberg, G. S. Large-scale diffusion barriers from CVD grown graphene. *Adv. Mater. Interfaces* **2**, 1500082 (2015).